Chapter 3

Synthesis of Multiwalled Carbon Nanotubes (MWCNT) and related carbon nanostructures

In this chapter, synthesis of MWCNT by chemical vapour deposition from renewable precursors was discussed. A total of six plant based oils (turpentine oil, sesame oil, soybean oil, sun flower oil, refined mustard oil, palmolein oil), one animal fat (ghee of cow's milk), one carbohydrate (D-fructose) and two alcohols (1- butanol, vinyl alcohol) were used as precursors for the production of CNTs and related carbon nanostructures such as nanowhiskers, nanorings etc. under catalyst free and catalytic conditions. Antioxidant efficacy and electrochemical behaviour of a few select synthesised materials were studied.

3.1. Introduction

Carbon nanotubes(CNTs) are either open or closed ended cylinders ofcarbon formed by the rolling of graphene like sheets andcan be classified intosingle layer boundary called single walled carbon nanotubes (SWCNTs) and whencylinders are formed from multiple layers having a hollow concentric assembly called multiwalled carbon nanotubes (MWCNTs). The report of multiwalled carbon nanotubes by Ijima *et al.* in 1991 generated worldwide enthusiasm about CNTs and their unique properties

enabled by their nanoscale structures spanning across academia and industry [1]. CNTs have developed into one of the most competitively studied nano-materials because of their exceptional structural features and excellent physical properties such as nanoscale low dimensionality, high aspect ratio, high mechanical strength [2-15], thermal conductivity [16-29] and remarkable electrical conductivity [30-44]. The one dimensionality of the nanotube structure has given rise to exceptional physical and chemical properties and potential applications in different fields such as structural composites [45], field emission [46-50], electrochemical device [51-54], molecular sensor [55-60], actuators [61,62], biomedical system [63-65], solar cells [66-68] and hydrogen storage [69-74]. Mass production and structure control of CNTs are key factors for realising industrial applications of CNT. Of the number of synthetic techniques, chemical vapour deposition (CVD) is the most efficient method for large-scale production of CNTs [75-77]. The ability to grow nanotubes directly on substrate using CVD technique allows the fabrication of high purity nanotubes in a controlled manner. This method provides reasonably good perspectives on large-scale and low-cost processes for the mass production of CNTs, a key point for their application at the industrial scale. Till date mostly fossil fuel based carbonaceous precursors such as methane, benzene, acetylene, ethanol, xylene etc. are being conventionally used as precursor for accessing CNTs which basically have non-renewable origin[78-81].These fossil fuel based carbon precursors are expensive, non-renewable and may be depleted in the near future [82]. Renewable plant based precursors have the potential to address such problems. The use of plant sources may be one of the better options for the industrial scale production of CNTs. Plant based precursors such as camphor, turpentine, neem and eucalyptus oil are also documented for production of CNTs via CVD method [83-86]. Recently, single-walled CNTs, MWCNTs and vertically aligned MWCNTs were accessed by this method using natural carbon feedstock [87-89]. Controlled synthesis of nanotubes thus unfolds newer possibilities particularly in the context of electromechanical properties and devices, chemical functionalization, surface chemistry, photochemistry etc. [90]. CNTs, often perceived as rolled up graphene sheets, owing to large arrays of conjugated double bonds can readily scavenge free radicals. As opposed to a staggering number of papers dealing with CNTs those which involve antioxidant activity of such materials are extremely scarce. Amazingly, only a few publications till date addressed the antioxidant activity of CNTs [91, 92]. The catalytic growth of CNTwas extensively reported by various

groupsusing transition metal and rare earth catalysts[93, 94]. The literature on catalyst free synthesis of CNTs are, however, scant.

The major aim of this chapter is the synthesis of CNT and related carbon nanostructures from renewable natural precursor under both catalytic (iron, nickel, cobalt nanoparticles) and catalyst free conditions and to explore their antioxidant efficacy and electrochemical behaviour.

3.2. Preparation of catalyst (iron, nickel and cobalt nanoparticles)

The metal nanoparticle catalyst was prepared in two-step process. First, the conversion of metal salts to metal oxide nanoparticles were achieved using urea (1:10 molar ratio) following solution combustion method [95]. The metal oxide so formed is reduced to metal nanoparticle under H_2 gas environment at 700^0C for 2 hours in a CVD furnace.

The scheme of synthesis may be represented as:

Step 1: Synthesis of metal oxide nano particles

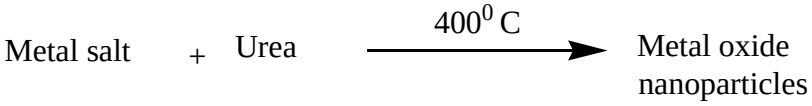

Metal salt: Urea =1:10

Metal salt: $Fe(NO_3)_3.9H_2O$, $Co(NO_3)_2.6H_2O$, $Ni(NO_3).6H_2O$

Step 2: Reduction of metal oxide nano particles by H_2 gas in CVD furnace

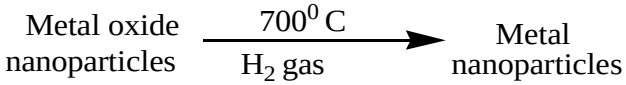

3.2.1.Transmission electron microscopy of catalyst

TEM micrographs (**Fig.3.1**) revealed non-uniform agglomerated nanoparticles. The particle size of iron nanoparticleswas found to be in the range of 30-35nm. The particle size of nickel nanoparticleswere in the range 5-15 nm and that of cobalt nanoparticles20-25nm.

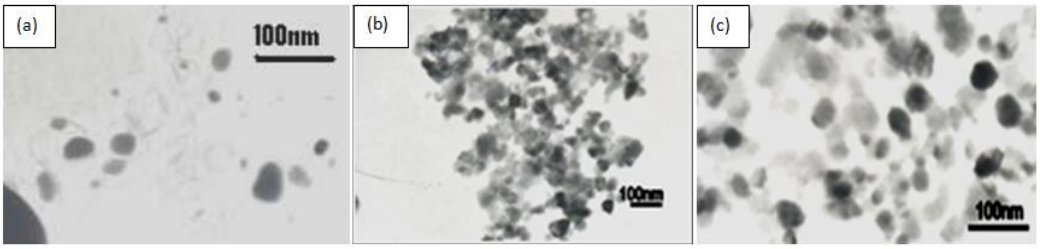

Fig.3.1.TEM images at magnification 100X of **(a)** Fe nanoparticles**(b)** Ni nanoparticles **(c)** Co nanoparticles

3.3. Multiwalled carbon nanotubes (MWCNT) from turpentine oil

3.3.1. Materials

Commercial turpentine oil is used as precursor for the synthesis of MWCNT. Turpentine oil is usually derived from the oleoresin of *Pinus palustris* of pinaceae family. The oil is used as thinner in paints and varnishes. Turpentine oil is a mixture of terpenes and essential oils such as such as α-pinene, β-pinene, carene, etc.which vary in percentage based in geographical location, tree species, and distillation process.

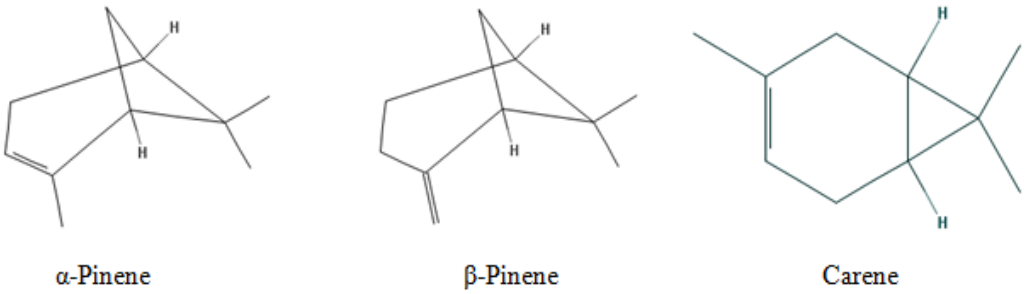

Fig.3.2. Chemical structure of major components of carbon source: turpentine oil

3.3.2. Synthesis of MWCNT from turpentine oil

(a) Catalyst free synthesis of MWCNT: The MWCNTs were prepared by chemical vapour deposition (CVD) method without using any external catalyst. A quartz boat loaded with turpentine oil(~10 g) was kept in a lower-temperature zone (300°C) and an empty quartz boat was kept at a higher temperature zone (700°C) in a horizontal quartz tube. Argon gas was then purged at a rate of 6cm^3/min. The furnace was heated to 700°C at a rate of 7°C /min for 2 hours and then allowed to cool to ambient temperature whereupon the CNTs were obtained as black powder (yield ~3.0 g).

(b)Synthesis of MWCNT using Fe nanoparticles as catalyst: The MWCNTs were prepared by CVD method using Fe nanoparticles as catalyst. A quartz boat loaded with turpentine oil(10 g) was kept in a lower-temperature zone (300°C) and another quartz boat in which 1mg of Fe nanoparticles previously dispersed uniformly using ethanol was kept at a higher temperature zone (700°C) in a 1m long horizontal quartz tube in the CVD furnace. Argon gas was then purged at a rate of $6cm^3$/min. The furnace was heated to 700°C at a rate of 7°C /min for 2 hours and then allowed to cool to ambient temperature whereupon the CNTs were obtained as black powder. In order to remove the catalyst, the synthesized CNT samples were treated with 6M HCland subsequent washing with deionised water[96]. The yield was recorded to be 3.3 g.

3.3.3. Results and discussion

The as obtained CNT black powders were found to be stable in air for months and can be dispersed in aqueous and organic solvents (methanol, ethanol) under ultrasonication. The yield of the CNTs was found to be 30-33% by weight of initial mass. Tap densities of the CNTs synthesized from turpentine oil with or without catalyst were calculated to be $0.26gcm^{-3}$ and $0.21gcm^{-3}$, respectively. Though the production of CNT from turpentine oil was extensively reported by different researchers at various experimental temperatures using Fe nanoparticle as catalyst by spray pyrolysis, however, catalyst free synthesis of MWCNT via chemical vapour deposition is scant [97, 98]. The catalyst free synthesis afforded micrometer long CNTs while catalytic condition results in shorter CNTs.

3.3.3.1. Scanning electron microscopy of CNT

The SEM micrograph (**Fig.3.3**) of the as-obtained material under catalyst free condition revealed the presence of spaghetti entangled bundles of micrometer length CNTs. The dense spontaneous packing of CNTs presumably occurs due to vander Waals' interaction between the carbon nanotubes.

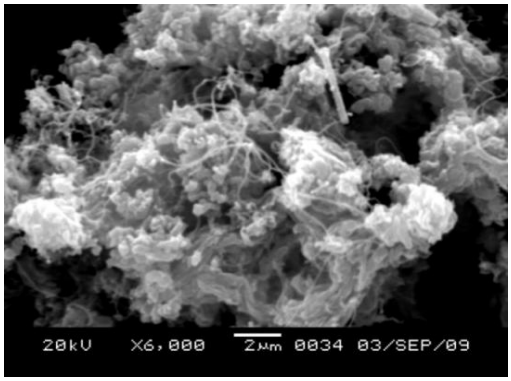

Fig.3.3. SEM micrograph of the as-obtained CNT

3.3.3.2. Transmission electron microscopy of MWCNT

Transmission electron microscopy is used to identify the correct phase of the CNT.The TEM micrographs (**Fig.3.4 (a, b))** of the as-obtained material under catalyst free condition, revealed the 8µm long multi-walled nanotubes. These CNTs have an empty and uniform central core. The HRTEM image (**Fig.3.4(c)**)of as-grown CNTs revealed the outer and inner diameters of 49 and 24nm, respectively. The selected area electron diffraction (SAED) pattern(**Fig.3.4 (d)**) taken from the CNTs showed the presence of sharp graphitic (002), (101) and (112) reflections.

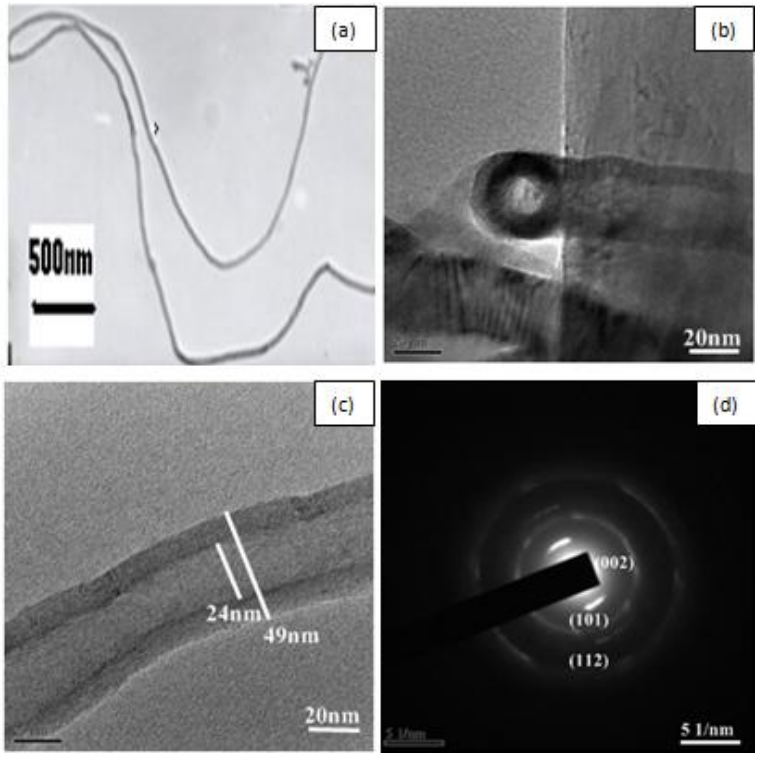

Fig.3.4. (a, b) TEM micrographs **(c)** HRTEM micrograph **(d)** SAED pattern of MWCNT obtained from turpentine oil under catalyst free condition

The TEM micrographs **(Fig.3.5 (a),(b))** of the as-obtained CNT using Fe nanoparticles as catalyst revealed shorter nanotubes as compared to that obtained under catalyst free condition. The HRTEMmicrograph **(Fig. 3.5 (c))** showed much smaller diameter of as-grown CNTs with outer and inner diameters 35.8 nm and 16.5nm, respectively. The interlayer distance is about 0.35 nm which resembles that of (002) plane of the graphitic carbon. Both circular rings typical of graphitic carbon and scattered spots originating from iron nanoparticles are visible in the SAED pattern (**Fig.3.5 (d)**).

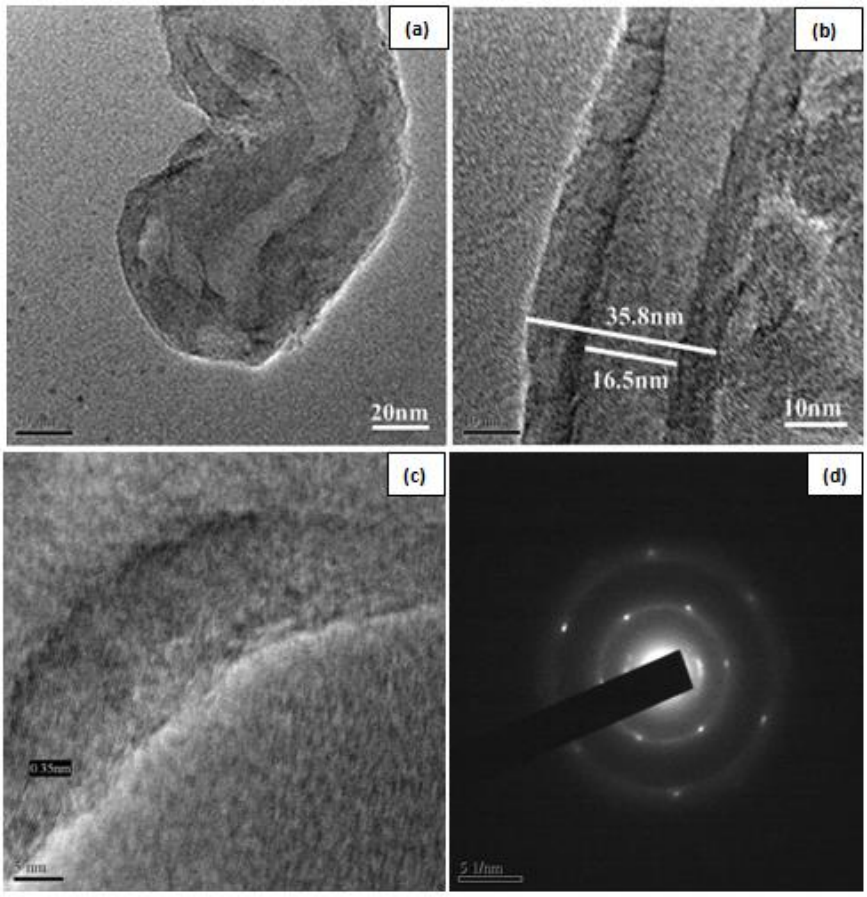

Fig.3.5. (a,b) TEM micrographs **(c)** HRTEM micrograph**(d)** SAED patternof MWCNT obtained under catalytic conditionfrom turpentine oil

3.3.3.3. X-ray diffraction study of MWCNT

The XRD pattern of the sample synthesized under catalyst free condition (**Fig.3.6**) revealed broad peaks. The peaks are indexed to be (002), (100), (101), (004) and (110) reflections of hexagonal graphitic carbon (JCPDS file No. 23-0064). The presence of the (002) peak in the XRD spectrum indicates the concentric cylindrical

nature of the graphene sheet nested together and the nanotubes are multi-walled in nature. The interlayer spacing (d_{002} = 0.34 nm) found from XRD is characteristic of CNTs. The average crystallite size(D) was estimated using the Debye-Scherrer equation, D= kλ /βCosθ, where k is Scherrer's constant, known as the shape factor and its value is taken as (0.89), λ is the wavelength of X-ray (λ=1.54056 Å), β is full width at half maximum (FWHM) (in radian) of the XRD peak and θ is the Bragg's angle. The average crystallite size was found to be 17.9nm.

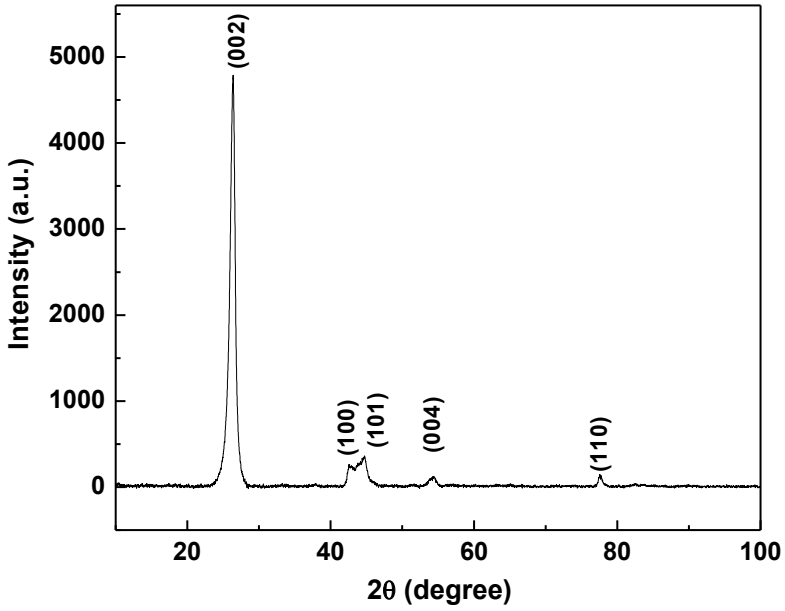

Fig.3.6.XRD pattern of MWCNT obtained from turpentine oil under catalyst free condition

The XRD pattern (**Fig.3.7**) of the as obtained CNTs using iron nanoparticles as catalyst revealeda number of intense and sharp peaks assigned toBragg reflections from both graphitic carbon and iron. The characteristic peaks for iron in XRD corroborated the presence of traces of catalyst in the sample.Theiron nanoparticles are believed to be encapsulated by graphitic layers during the formation of CNTs [99]. The peaks are indexed to be (002), (100), (101), (102), (004) and (103) reflections of hexagonal graphite (JCPDS file No. 23-0064) and (100), (200), (211), (220), (301), (222) and (321) crystallographic planes of cubic iron (JCPDS file no.01-1267). The average crystallite size estimated by the Debye-Scherrer equation using a Gaussian fit was found to be62.4nm for (002) plane of graphite. The sharp peaks indicated that

higher purity of as-grown CNTs compared to that obtained under catalyst free conditions.

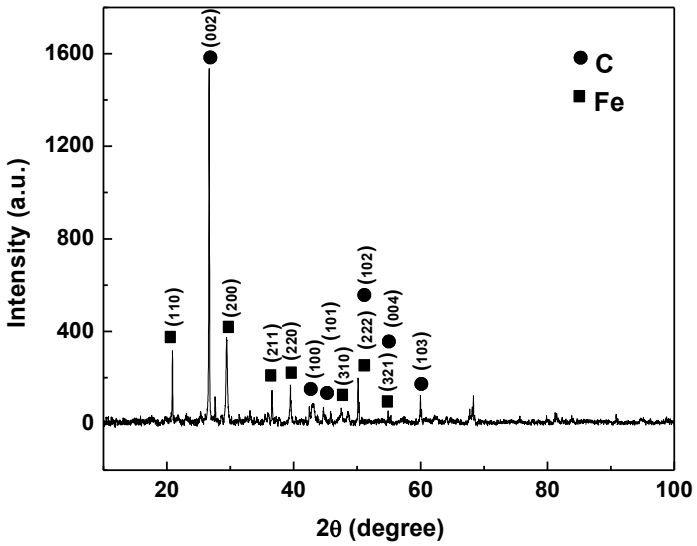

Fig.3.7.XRD pattern of MWCNT obtained from turpentine oilusing catalyst

3.4. Spiral multiwalled carbon nanotubes (MWCNT) and carbon nanowhiskers (CNW)from sesame oil

3.4.1. Materials

Commercial sesame oil (locally called til oil)is usedas precursor for the synthesis of spiral MWCNT and CNW. Sesame oil is composed of linoleic acid (41%), oleic acid (39%), palmitic acid (8%), stearic acid (5%) and others fatty acids in small amounts. Sesame oil is polyunsaturated semi-drying oil. Commercial sesame oil varies in colour from light to deep reddish yellow depending on the colour of the seed processed and the method of milling.

Fig.3.8. Photograph of sesame oil

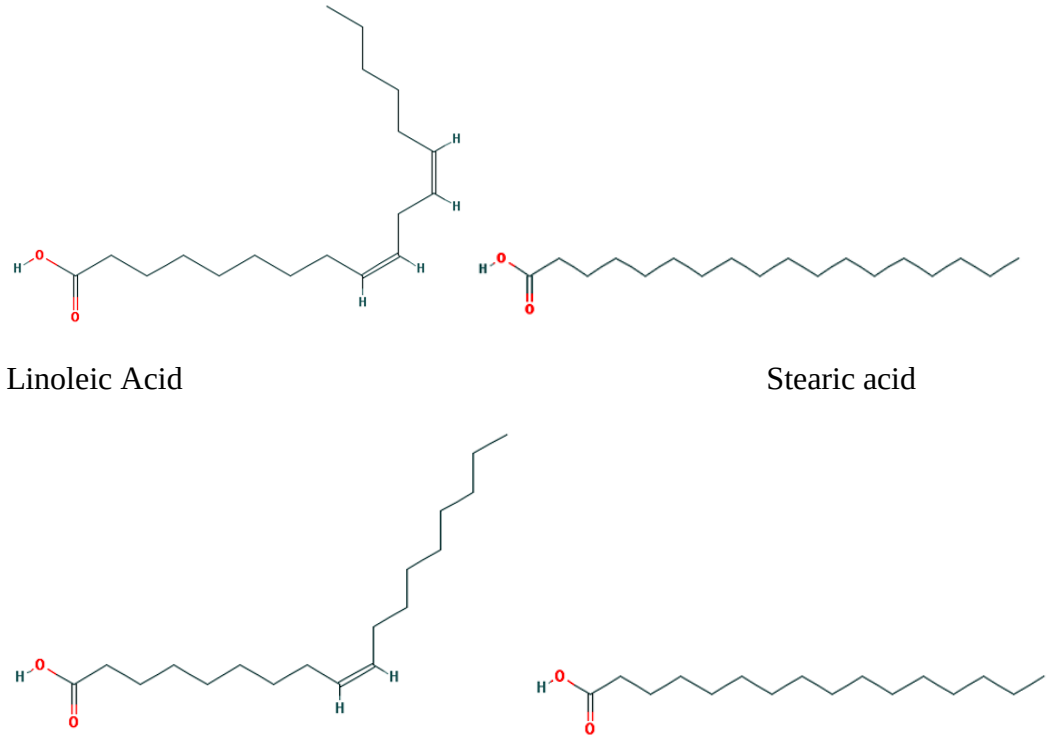

Fig.3.9. Chemical structure of major components of carbon source: sesame oil

3.4.2. Synthesis of spiral MWCNT and CNW from sesame oil

(a) Synthesis of spiral MWCNT: The spiral MWCNT was prepared by chemical vapour deposition under catalyst free condition. A quartz boat loaded with sesame oil (~10 g) was kept in a lower-temperature zone (300^0C) and an empty quartz boat was kept at a higher temperature zone (600^0C) in a horizontal quartz tube in a CVD chamber. Argon gas was then purged at a rate of $6cm^3$/min. The furnace was heated to 600^0C at a rate of 7^0C /min for 2 hours and then allowed to cool to ambient temperature whereupon the CNTs were obtained as black powder (yield ~2.8 g).

(b)Synthesis of CNW: The CNWs were prepared using Ni nanoparticle as catalyst by CVD method. A quartz boat loaded with sesame oil (~10 g) was kept in a lower-temperature zone (300^0C) and another quartz boat in which 1mg of Ni nanoparticles were spread using dispersion in ethanol was kept at a higher temperature zone (600^0C) in a horizontal quartz tube. Argon gas was then purged at a rate of $6cm^3$/min. The furnace was heated to 600^0C at a rate of 7^0C /min for 2hours and then allowed to

cool to ambient temperature whereupon the CNWs were obtained as black powder (yield ~3 g).

3.4.3. Results and discussion

The as obtained CNT and CNW black powder were found to be stable in air for months and can be dispersed in aqueous and organic solvents (methanol, ethanol) under ultrasonication. The yield of the materials was found to be 28-30% by weight of initial mass. The catalyst free synthesis afforded spiral carbon nanotubes whereas catalytic condition resulted in carbon nanowhiskers.

3.4.3.1.Transmission electron microscopy of spiral MWCNT

The TEM micrographs (**Fig.3.10 (a,b)**) of the as-obtained CNTsfrom sesame oil without using catalyst revealedthe presence of >3μm long hollow spiral multiwalled carbon nanotubes. The sheets of graphenes are orderly arranged in concentric cylinders. HRTEM suggested the as-grown nanotubes to be consisting of concentrically nested ~ 45 graphene sheets. The outer and inner diameters of the nanotubes were 54.68 and 22.94 nm, respectively and the tubes were open ended. The interlayer distance is about 0.33 nm which resembles (002) plane of the graphitic carbon(**Fig.3.10 (g) (h)**). The SAED pattern (**Fig. 3.10(f)**) revealed concentric rings that are characteristic of (002), (101), (113) planes of graphitic carbon.

Spiraled nanotubes are believed to have more interesting applications than their straight counterparts [100]. Conduction of electricity through coiled nanotubes can generate an inductive magnetic field are relevant in electromagnetic nano-transformers or nano-switches. Spiraled nanotubes may also serve as mechanical components such as resonating elements, nano-springs, high-performance electromagnetic absorbers, and nano-actuators especially the vertically straight portion of a zigzag shaped nanotube, can serve as a high-resolution nanotube scanning tip with the bent portion making enhanced bonding to the AFM pyramid sidewall [101]. Their spiral shape induces mechanical interlocking when the composites are subjected to loading [102-103].

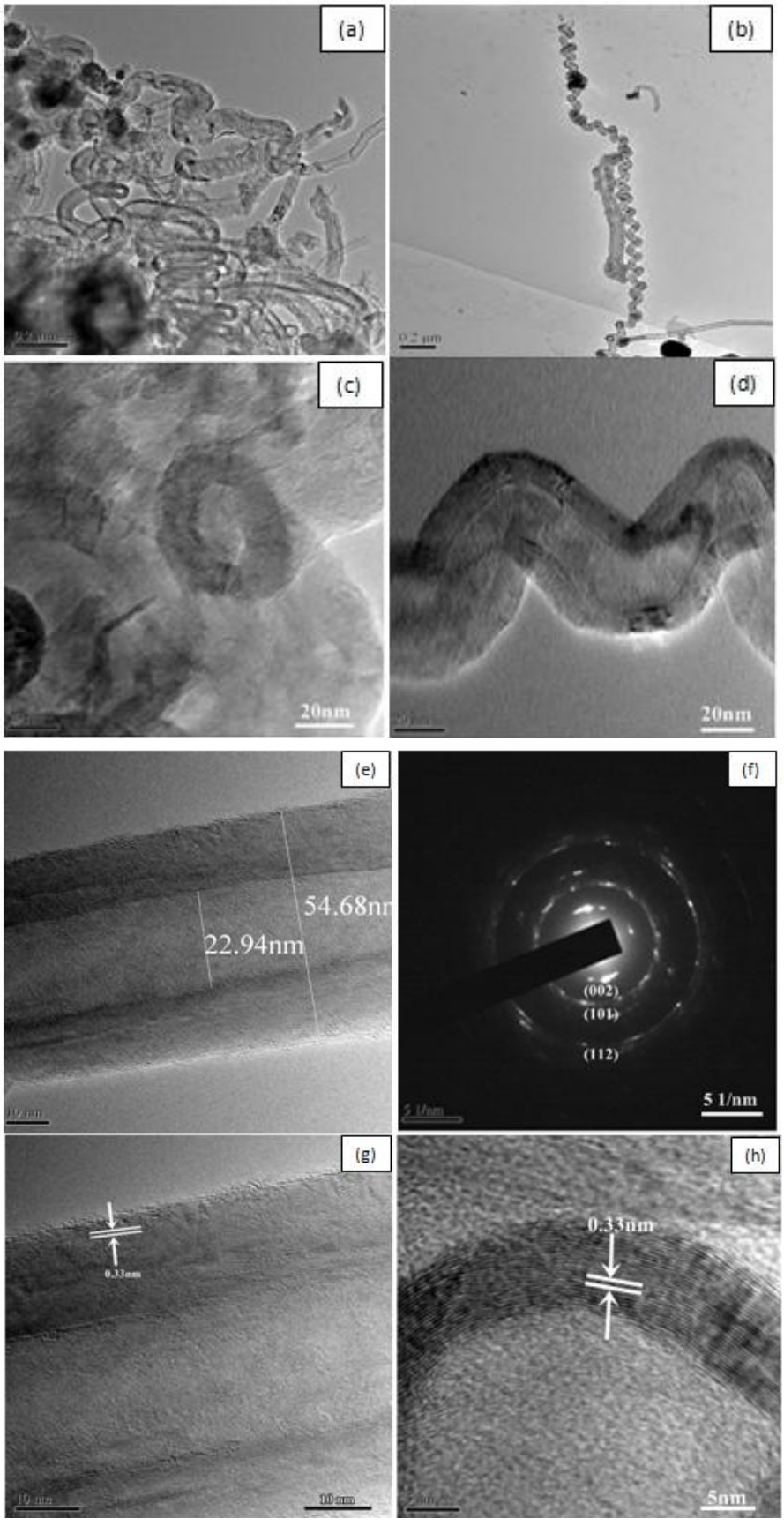

Fig.3.10. (a, b) TEM micrographs **(c-e,g,h)** HRTEMmicrographs **(f)** SAED pattern of spiral MWCNT obtained from sesame oil

3.4.3.2.Scanning electron microscopy and transmission electron microscopy of carbon nanowhiskers (CNW)

The SEM micrographs (**Fig.3.11 (a)**) showed the presence of bundles of carbon nanowhiskers. The TEM image **(Fig.3.11(b), (c))** revealed entangled carbon nanowhiskers. As can be seen from both SEM and TEM micrographs, the as-grown bundles of CNWs are clean and free from other carbonaceous materials.The low magnification image indicated the solid filamentous structure without any hollow tubular growth.

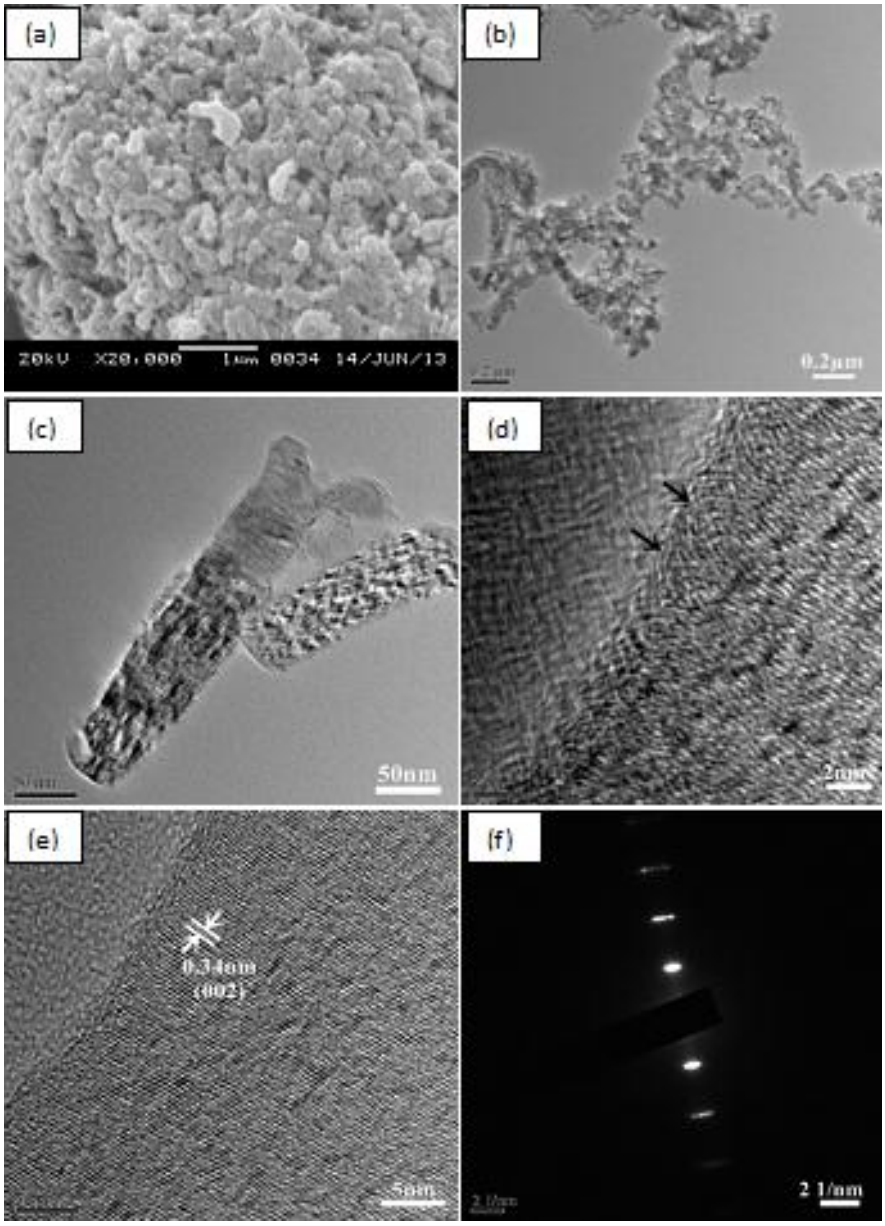

Fig.3.11 (a) SEM micrograph **(b,c)** TEM micrographs **(d,e)** HRTEM micrographs **(f)** SAED pattern of CNW from sesame oil

The HRTEM image pointed the graphitized nature (**Fig.3.11 (e)**) of the nanowhiskers with carbon spiralsindicated by black arrows(**Fig.3.11(d)**) arranged perpendicular to the whisker axis. The spacing between two adjacent layers isabout 0.34nm and the diameter of the whiskers is found to be 60-80nm.The SAED pattern (**Fig.11 (f)**) revealedthe poly crystalline nature of the material.Dilute acid washed catalyst free nanowhiskers were found to have very little toxicity to mammalian cells and can be localized inside the cell nucleus thussuggesting their viability as potential delivery vehicles into the mammalian cells [104].

3.4.3.3. Probable mechanism of growth of carbon nanowhiskers

Based on experimental observation as reported in literature and tentative arguments, a probable mechanism for the formation of CNW has been proposed. The stepwise decomposition of the fatty acids present in the natural oils to gaseous constituents in presence of catalyst at 300 to 600^0 C followed by cooling to ambient temperature led to the formation of CNWs. At 300^0C under autogenic pressure, the polyunsaturated fatty acids present in oils decomposed to hydro peroxides and finally to carboxylic acid [105-107]. The long chain fatty acids also broke down to lower aliphatic chains fatty acids and hydrocarbons. On increasing the temperature further up to 500^0 C, the fatty acids are decomposed to lower hydrocarbons along with CO and CO_2. At a temperature 500 - 600^0C, the catalyst surface facilitated partial decomposition of the hydrocarbon and carbon oxides to elemental gaseous carbon along with molecular hydrogen and oxygen [108,109] thereby raising the gaseous pressure [110] inside the furnace. The CNW formation occurred at the desired temperature followed by cooling to ambient conditions. The pressure-driven deposition of gaseous carbon at the interface of substrate and catalyst is believed to be responsible for spiraled filamentous structure.

3.4.3.4. Powder X-ray diffraction study of MWCNT and CNW from sesame oil

The powder XRD pattern of as- obtained MWCNTfrom catalyst free CVD of sesame oil is shown in **Fig.3.12.** A number of strong Bragg reflections were obtained in the pattern of MWCNT corresponding to the (002), (100), (101), (102),(004) and (103) reflections of hexagonal graphitic carbon (space group $P6_3/mmc$, JCPDS Card No. 23-0064). The broad nature of the peaks indicatedreduced crystallite size with hardly

any long-range order. The average crystallite size estimated using a Gaussian fit was found to be 7.5nm.

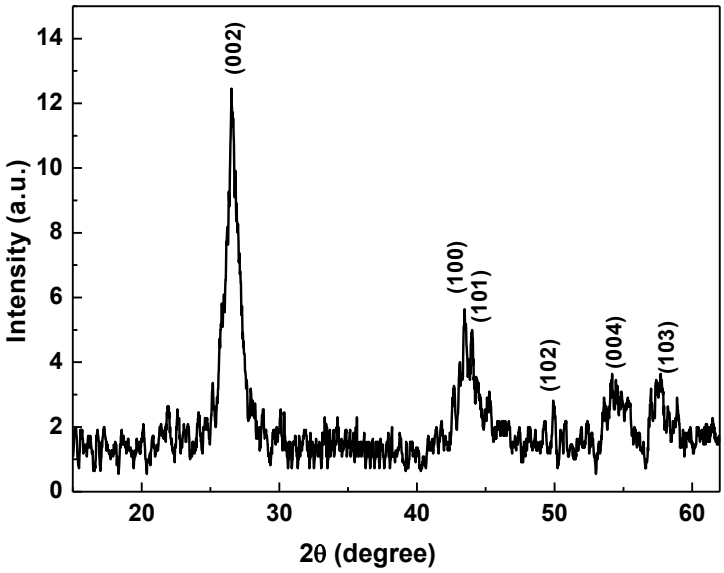

Fig.3.12.XRD pattern of MWCNT obtained from sesame oil (catalyst free)

The XRD pattern of CNW (**Fig.3.13)**from sesame oil using nickel nanoparticles as catalystexhibited a number of intense and sharp peaks assigned toBragg reflections from both graphitic carbon and nickel. Remnants of metal catalyst particleswere foundentrenched in the CNW.The X-ray diffraction pattern showed peaks at of 2θ values 43.90^0, 51.76^0 and 76.21^0correspond to the (111), (200) and (220) crystallographic planes of fcc Ni (JCPDS file no.04-0850) and peaks at 26.27^0, 44.35^0 and 51.20^0correspond to the (002), (101) and (102) crystallographic planes of hexagonal graphitic carbon (JCPDS file no. 23-0064). The interlayer spacing (d_{002} =0.33nm) from XRD, similar to that of graphitic carbon (0.33nm), showed orderly stacking.The average crystallite size estimated by the Debye-Scherrer equation using a Gaussian fit was found to be 7.8 nm for (002) plane of graphite.In contrast to the uncatalysed product, the carbon nanomaterials obtained undercatalytic conditionshowed higher degree of mono-dispersity.

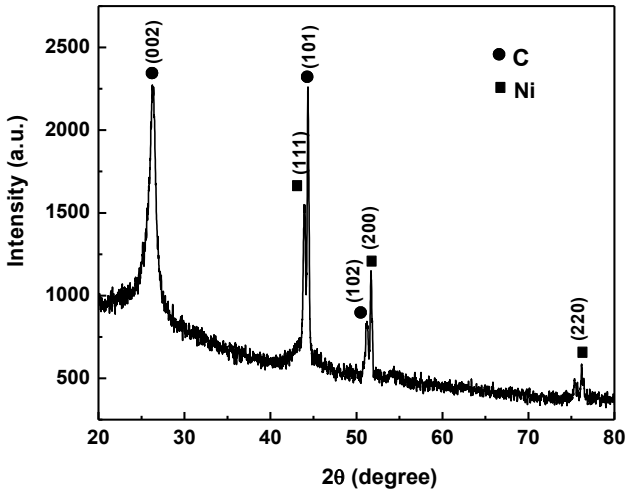

Fig.3.13.XRD pattern of CNWfrom sesame oil using catalyst

3.4.3.5. Antioxidant activity of MWCNT from sesame oil

The antioxidant activity of the MWCNT was assessed using a modified DPPH method for insoluble solids[111] by UV-visible spectroscopy noting the colour change from purple to yellow. DPPH is a stable free radical and accepts an electron or hydrogen radical to become a stable diamagnetic molecule. The reduction capability of DPPH radical is determined by the decrease in absorbance at 517 nm induced by antioxidants. The nanocomposite materials have the ability to reduce the stable radical DPPH to the yellow-coloured2,2-diphenyl-1-picrylhydrazine. DPPH radicals react with suitable reducing agent, the electrons become paired off and the solution loses colour stoichiometrically depending on the number of electrons taken up. An amount of 4 mg powdered sample was taken in a test tube and treated with 3 mL, 100 µM methanolic solution of DPPH. To enhance the surface reaction between the MWCNT material and the DPPH, the mixture was sonicated and kept in the dark for 15 minutes. After centrifugation at 10000 rpm, the optical absorptions of the supernatant was monitored at 517 nm. A DPPH control was also measured as reference. The aforementioned procedure was followed to ascertain time dependent DPPH scavenging at periodic interval of 5, 15, 30, 45 and 60 minutes.The percentage scavenging was calculated using the formula:

$$\text{DPPH scavenging (\%)} = [(A_c - A_s)/A_c] \times 100$$

where A_C and A_S are absorbances of the control DPPH and DPPH with the MWCNT at 517 nm respectively. The observed antioxidant activity was attributed to the

neutralisation of free radical character of DPPH by transfer of an electron as depicted in **Fig.3.14**. For evaluating SC-50 (the amount of samples required to scavenge 50% of DPPH), a similar procedure was adopted for 2, 4, 6, 8 and 10 mg of the MWCNT and absorbances recorded after 30 minutes.The control DPPH does not show any change of absorbance with time. However DPPH with MWCNT showed a steady decrease of absorbance at 517 nm(**Fig.3.15(a-e)).**The DPPH scavenging percentage can be calculated from decline in absorbance at 517 nm, which corresponds to the quantity of DPPH in methanolic solution. It is clear from the **Fig.3.15(c)** that after 30 minutes more than 50% of the DPPH was scavenged for 6mg of the MWCNT. The SC-50 value was ascertained graphically (**Fig.3.15 (f))** and was foundto be 4.83 mg.

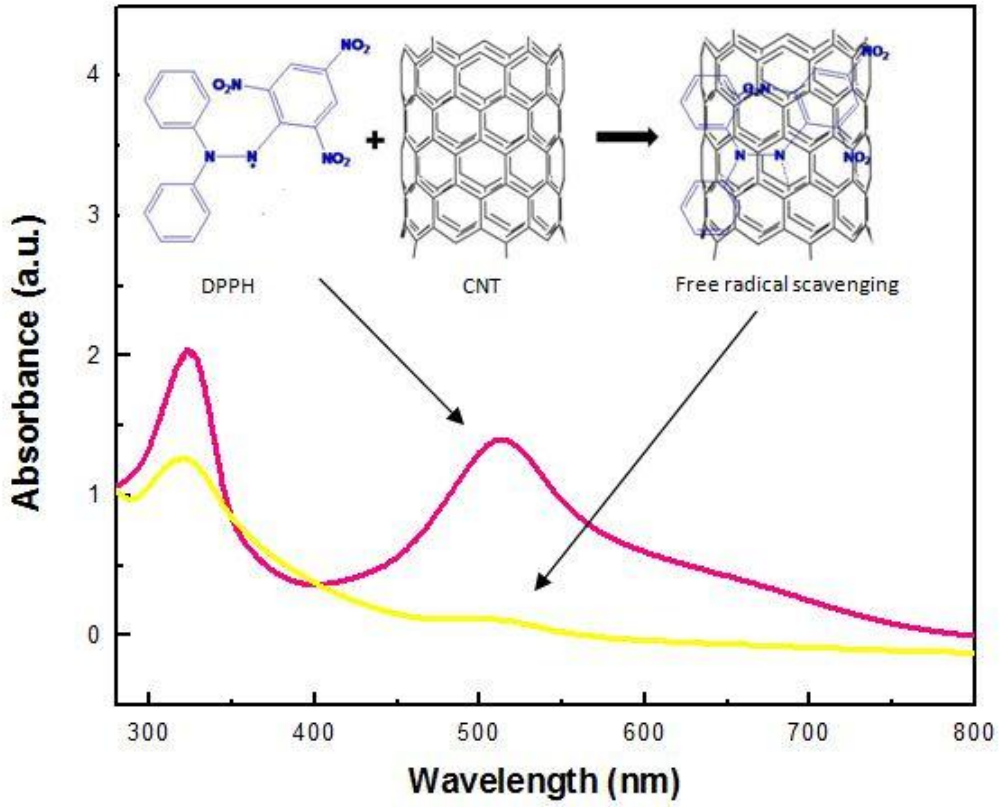

Fig.3.14.UV-visible spectra (DPPH scavenging)

Fullerenes being pool of pi electrons are expected to easily cope with a lack or excess of electrons and hence often referred to as electron sponges [112,113]. Carbon nanotubes embrace large arrays of conjugated double bonds and therefore they are expected to show significant electron donor and acceptor capabilities [92]. Accordingly, due to their unique structural feature and high pi electron density, it is

presumed that the MWCNT transfers its electron density to thefree-radical DPPH which might be responsible for its antioxidant efficacy (**Fig.3.14**).

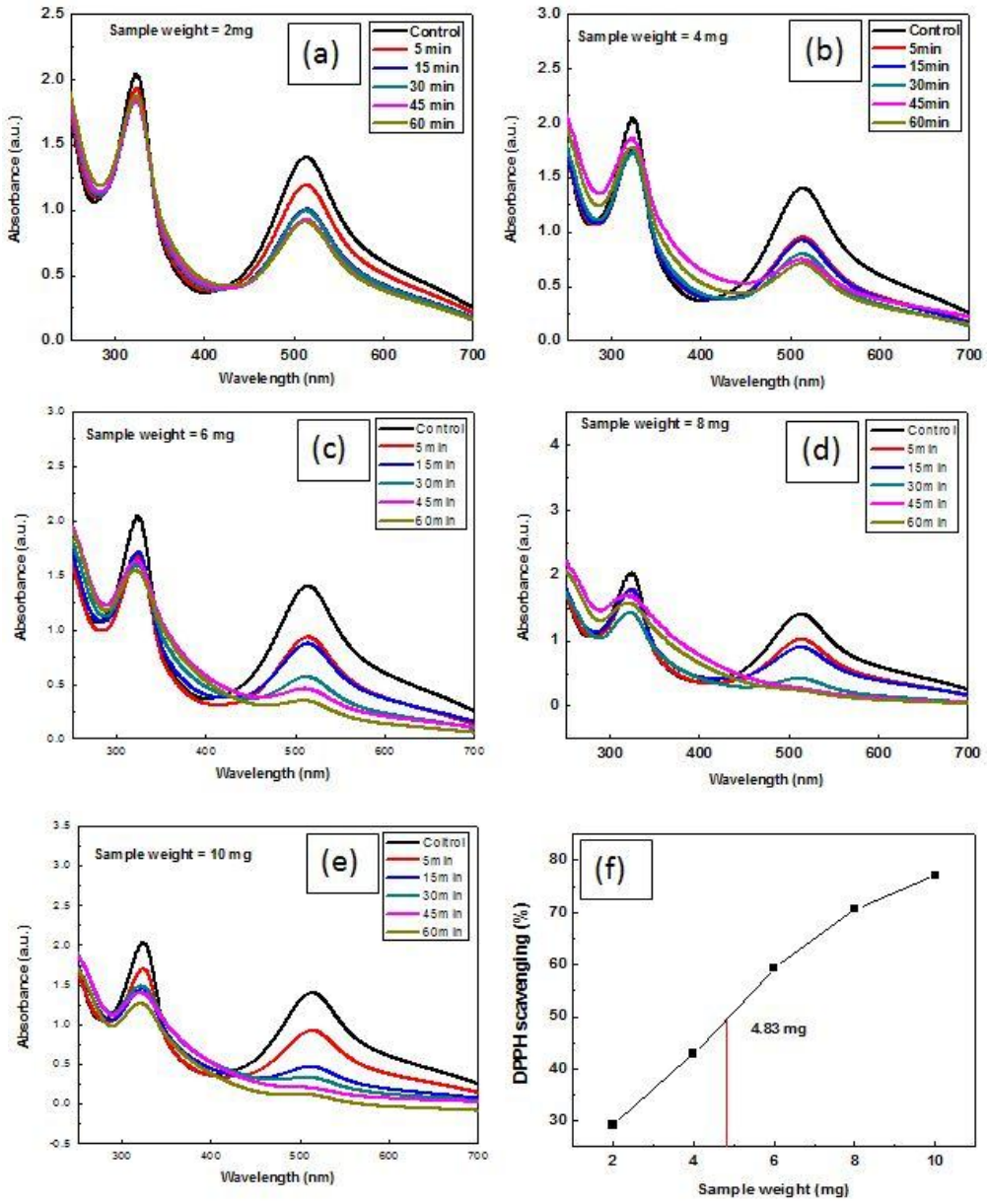

Fig.3.15. (a-e) Time dependent DPPH scavenging by varying MWCNT concentration**(f)** DPPH scavenging (%) at different weight of MWCNT

3.5. Multiwalled carbon nanotubes(MWCNT) from soybean oil

3.5.1. Materials

Soybean oil is used as carbon precursor for the synthesis of MWCNT. Soybean oil is a vegetable oil extracted from the seeds of the soybean (*Glycine max*)and often has a dark yellow or faint green colour. It is one of the most widely consumed cooking oil.

There arefour phytosterols: stigmasterol, sitosterol, campesterol and brassicasterolin soybean oil.Compositionally, per 100 g of soybean oil, there is about 14 g of saturated fat, 23 g of monounsaturated fat, and 58 g of polyunsaturated fat.The unsaturated fatty acids, linoleic acid, a type of omega-6 fat, is about 50 percent, and linolenic acid is about seven percent.

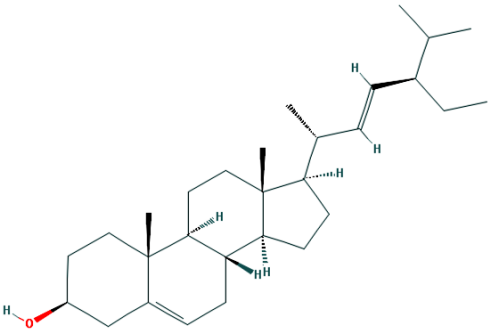

Stigmasterol

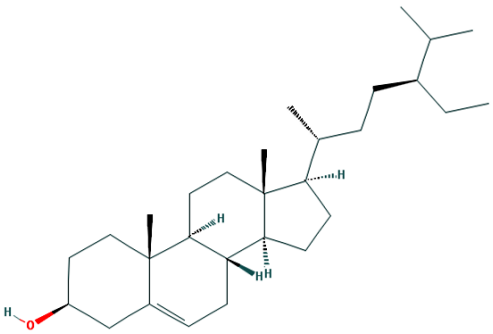

Sitosterol

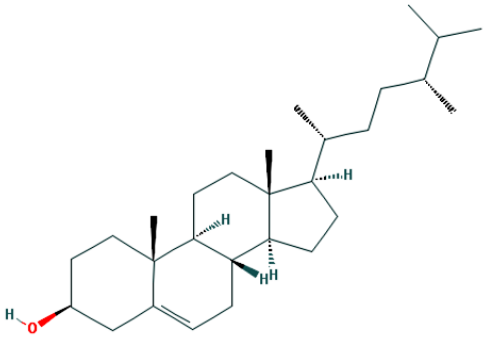

Campesterol

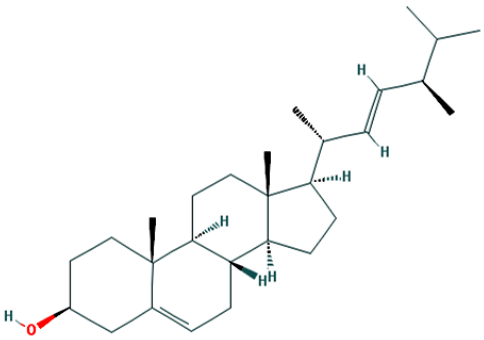

Brassicasterol

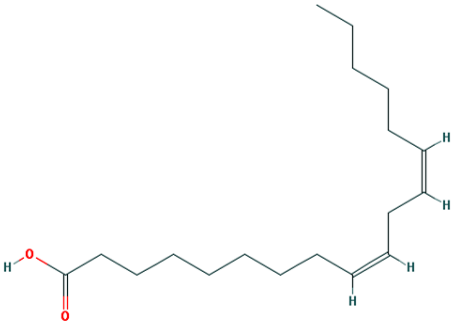

Linoleic acid

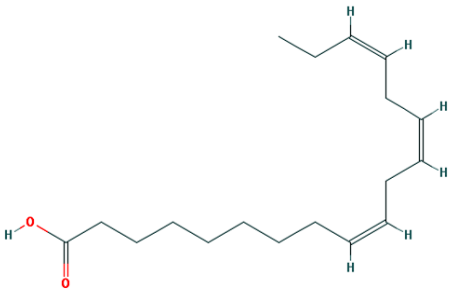

Linolenic acid

Fig.3.16. Chemical structure of major components of carbon source: soybean oil

3.5.2. Synthesis of MWCNT from soybean oil

The MWCNTs were prepared from soybean oilunder both catalyst free and catalytic conditions by CVD method in separate experiments. A quartz boat loaded with soybean oil (~10 g) was kept in a lower-temperature zone (300°C) and an empty quartz boat (for catalyst free synthesis) or quartz boat filled with 1mg of Ni nanoparticles previously dispersed uniformly in ethanol (for catalytic synthesis) was kept at a higher temperature zone (650^0C) in a horizontal quartz tube. Argon gas was then purged at a rate of 6cm^3/min. The furnace was heated to 650^0C at a rate of 7^0C /min for 2hour and then allowed to cool to ambient temperature whereupon the CNTswere obtained as black powder. The catalyst was removed by acid treatment following the standard procedure [115]. The yield was recorded to be 2.9g and 3.4 g, respectively.

3.5.3. Results and discussion

The as obtained CNT black powders were found to be air stable and can be dispersed in aqueous and organic solvents (methanol, ethanol) under ultrasonication. The CNT obtained from soybean oilafforded relatively good yield (34%) under catalytic condition as compared to catalyst free condition(29%).

3.5.3.1.Transmission electron microscopy of MWCNT from soybean oil without using catalyst

The TEM micrographs (**Fig.3.17 (a,b)**) revealed quasi-alignedclean uniform>10μm long hollow nanotubes. These CNTs have an empty and uniform central core and open at one end (**Fig. 3.17 (c-e)**). The HRTEM image (**Fig. 3.17 (f)**) revealed that the CNTs produced were multi-walled CNTs consisting of approximately 35 layers with inner and outer diameters of 19.43 and 44.81nm, respectively.They have long-range uniformity in the diameter.The interlayer distance is about 0.33 nm which resembles that of (002) plane of the graphitic carbon (**Fig. 3.17 (g)**). Undesirable structures like amorphous carbon are negligible. The SAED pattern (**Fig.3.17(h)**)revealed concentric rings that are characteristic of graphitic carbon.

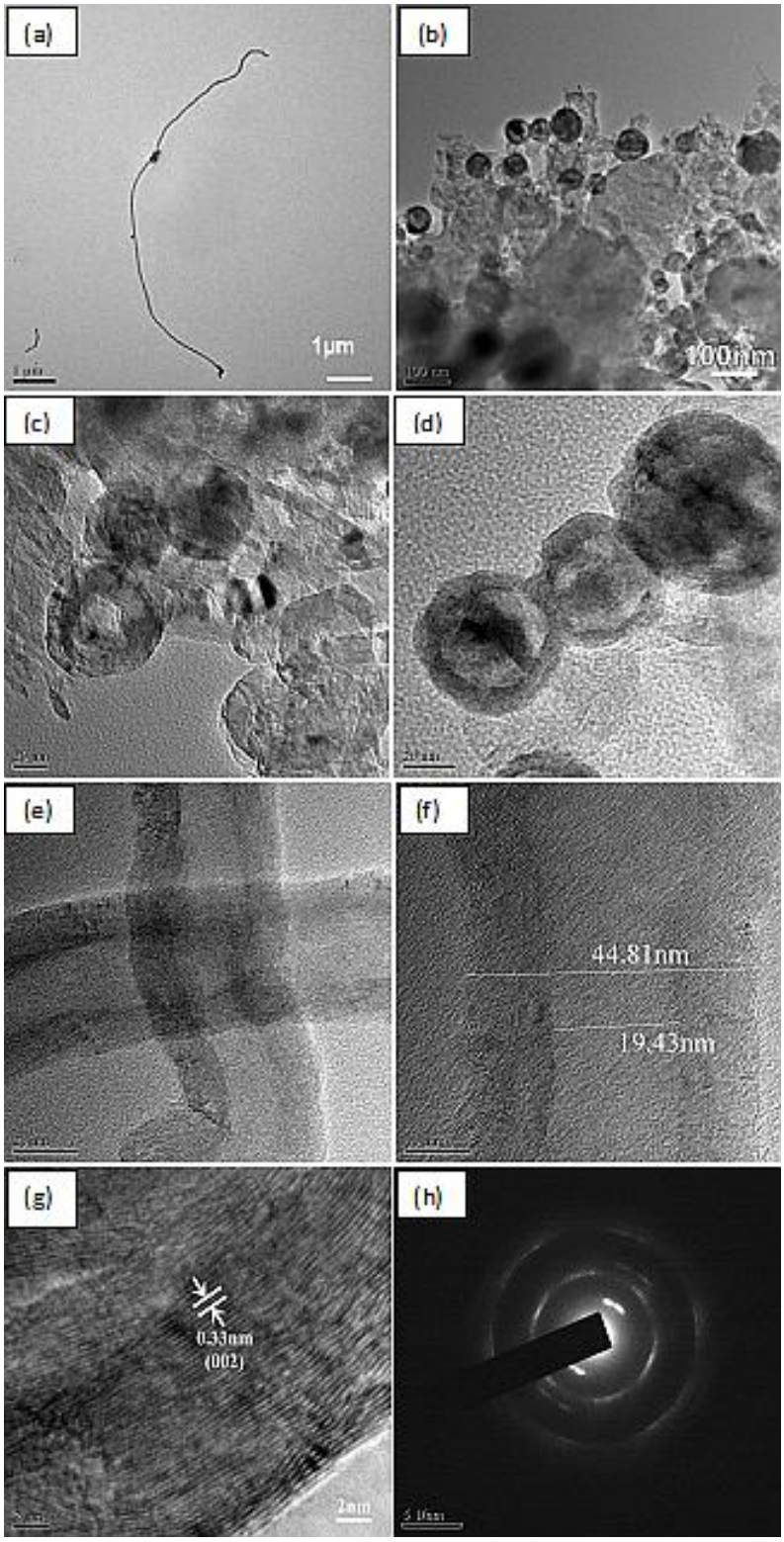

Fig.3.17.(a-e) TEM micrographs **(f, g)** HRTEMmicrographs **(h)** SAED pattern of MWCNT obtained from soybean oil without using catalyst

3.5.3.2.Scanning electron microscopy and transmission electron microscopy of MWCNT from soybean oil using nickel catalyst

The SEM micrographs (**Fig.3.18 (a)**) revealed bundles ofagglomerated nanotubes. The TEM image (**Fig. 3.18 (b)**) showed the structural defects in the as- grown CNT. The outer and inner diameters of the nanotubes were found to be 40.29 and 12.03 nm, respectively. HRTEM (**Fig. 3.18 (c)**) suggested the as-grown nanotubes to be consisting of concentrically nested ~ 39graphene sheets The lattice fringes between two adjacent planes are 0.34nm apart, which resembles the interlayer distance of (002) plane of the graphitic carbon. The SAED (**Fig. 3.18 (d)**) revealed concentric rings that are characteristic of graphitic carbon. The MWCNTs are neither aligned to particular direction nor do they have long-range uniformity in the diameter. Undesirable structures like amorphous carbon are negligible albeit with some structural defects.

It is noteworthy that number of graphene sheets rolled to form the MWCNTs almost remain the same in both catalyst free (35) and catalytic synthesis (39).

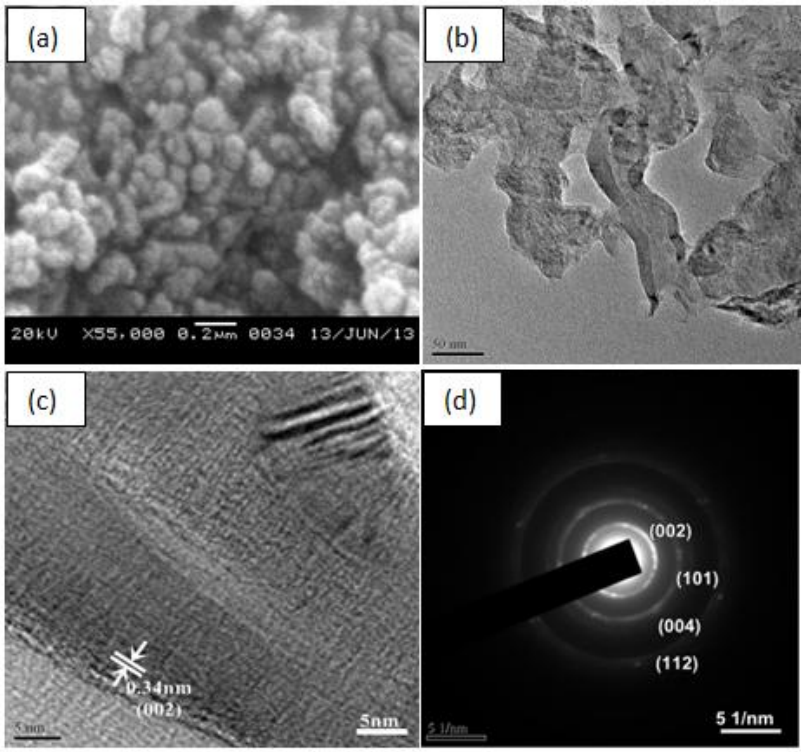

Fig.3.18. (a) SEM micrograph **(b)** TEM micrograph **(c)** HRTEM micrograph **(d)** SAED pattern of MWCNT obtained from soybean oil using Ni catalyst

3.5.3.3. Powder X-ray diffraction study of MWCNT from soybean oil (catalyst free)

The powder XRD pattern of the synthesized MWCNTs under catalyst free condition from soybean oil is shown in (**Fig.3.19**). A number of strong Bragg reflections were obtained in the pattern corresponding to the (002), (101), (102), (004) and (103) reflections of hexagonal graphitic carbon (JCPDS Card No. 23-0064, space group $P6_3/mmc$). The average crystallite size estimated by the Debye-Scherrer equation, $d=k\lambda/\beta\cos\theta$ using a Gaussian fit was found to be 10.0 nm.

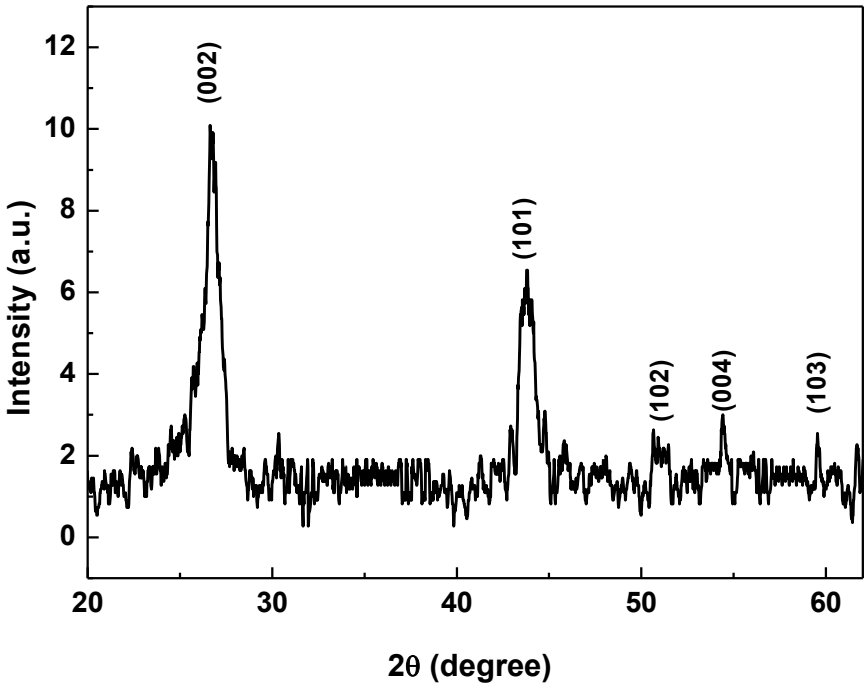

Fig.3.19.XRD pattern of MWCNT obtained under catalyst free condition from soybean oil

The XRD pattern **(Fig.3.20)** of the synthesised MWCNTfrom soybean oil using nickel nanoparticles as catalyst exhibited intense and sharp peaks assigned toBragg reflectionsof graphitic carbon and nickel. The X-ray diffraction pattern showed peaks (44.75^0 and 51.76^0) of 2θ values ranging from 10^0 to 70^0, which correspond to the (111) and (200) crystallographic planes of fcc Ni (JCPDS file no.04-0850) and peaks (26.42^0, 44.58^0 and 51.53^0) of 2θ values also correspond to the (002), (101) and (102) crystallographic planes of hexagonal graphitic carbon (JCPDS file no.23-0064). The

interlayer spacing (d_{002} = 0.338nm) from Bragg's equation, similar to that of graphite (0.335nm), showed orderly stacking in the MWCNT. The average crystallite size estimated by the Debye-Scherrer equation using a Gaussian fit was found to be 7.8nm for (002) plane of graphite. The presence of nickel can be attributed to the fact that the catalyst particles were either remained inside the nanotubes channels or encapsulated by graphitic layers during synthesis of CNT.

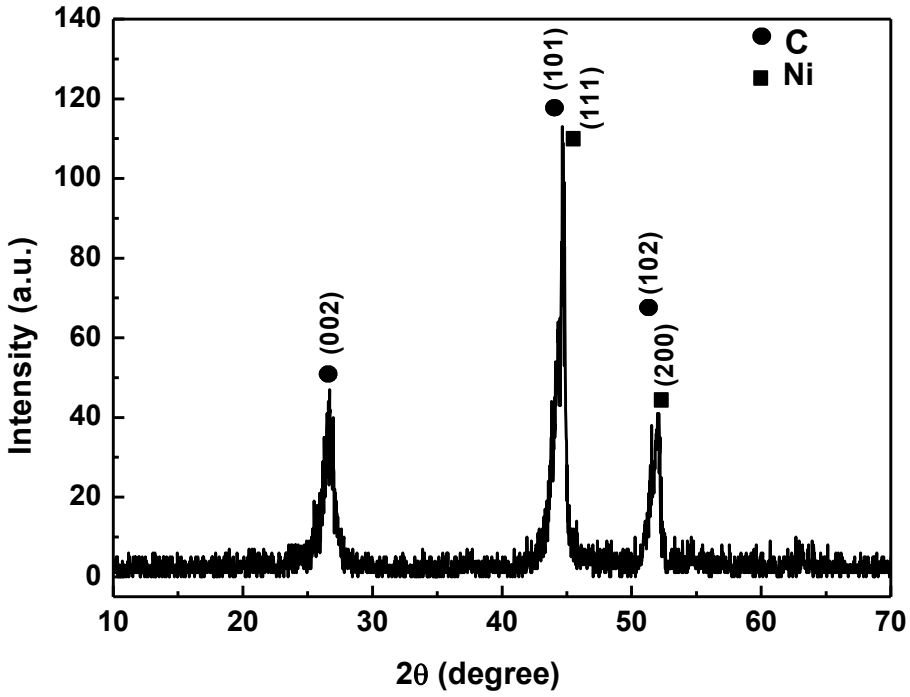

Fig.3.20. XRD pattern of MWCNTobtained using Ni catalyst from soybean oil

3.6. Multiwalled carbon nanotube(MWCNT) from sunflower oil

3.6.1. Materials

Sunflower oil is used as carbon source for the synthesis of MWCNT.Sunflower(*Helianthus annuus*) oil is the non-volatile oil compressed from sunflower seeds. It is mostly oleic acid (omega-9)-linoleic acid (omega-6) group of oils. The oil is of light amber colour with a mild and pleasant flavour, refined oil is pale yellow.The oil contains appreciable quantities of vitamin E, sterols, squalene and other aliphatic hydrocarbons. Sunflower oil is commonly used in food as frying oil and in cosmetics.

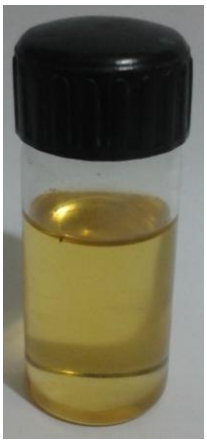

Fig.3.21. Photograph of sunflower oil

3.6.2.Synthesis of MWCNT from sunflower oil

The MWCNTs were prepared by CVD method from sunflower oil using Ni nanoparticlesas catalyst following similar synthetic procedure discussed in the section **3.3.2.** of this chapter. The as obtained products were treated with mild acid as well as base in order to remove the catalyst. The yield was recorded to be 2.6g.

3.6.3.Results and discussion

The as obtained CNT from sunflower oil using nickel nanoparticle as catalyst was found to be stable in air for months and can be dispersed in aqueous and organic solvents (methanol, ethanol) under ultrasonication. The yield of the materials was found to be 26% by weight of initial mass. The catalyst free chemical vapour deposition of sunflower oil under similar conditions afforded agglomerated product.

3.6.3.1.Scanning electron microscopy and transmission electron microscopy

The SEM micrograph (**Fig.3.22 (a)**) revealed the presence of bundles of entangled nanotubes.The dense-spontaneous packing of CNTs occurs due to vander Waals' interaction between the carbon nanotubes.The TEM micrographs (**Fig. 3.22 (b-d)**) revealed bundles of entangled multiwalled carbon nanotubes with outer and inner diameters of the nanotubes33.6 and 8.6 nm, respectively. HRTEM (**Fig. 3.22 (e))** suggested the as-grown nanotubes to be consisting of concentrically nested ~ 40graphene sheets. The interlayer distance is 0.34 nm which resembles that of (002) plane of the graphitic carbon. The darkblack spotsin HRTEM images are ascribedto themetal catalyst particles embedded within the carbon nanotubes. The SAED pattern

(**Fig. 3.22 (f)**) revealed concentric rings that are characteristic of graphitic carbon and polycrystalline nature of the material.

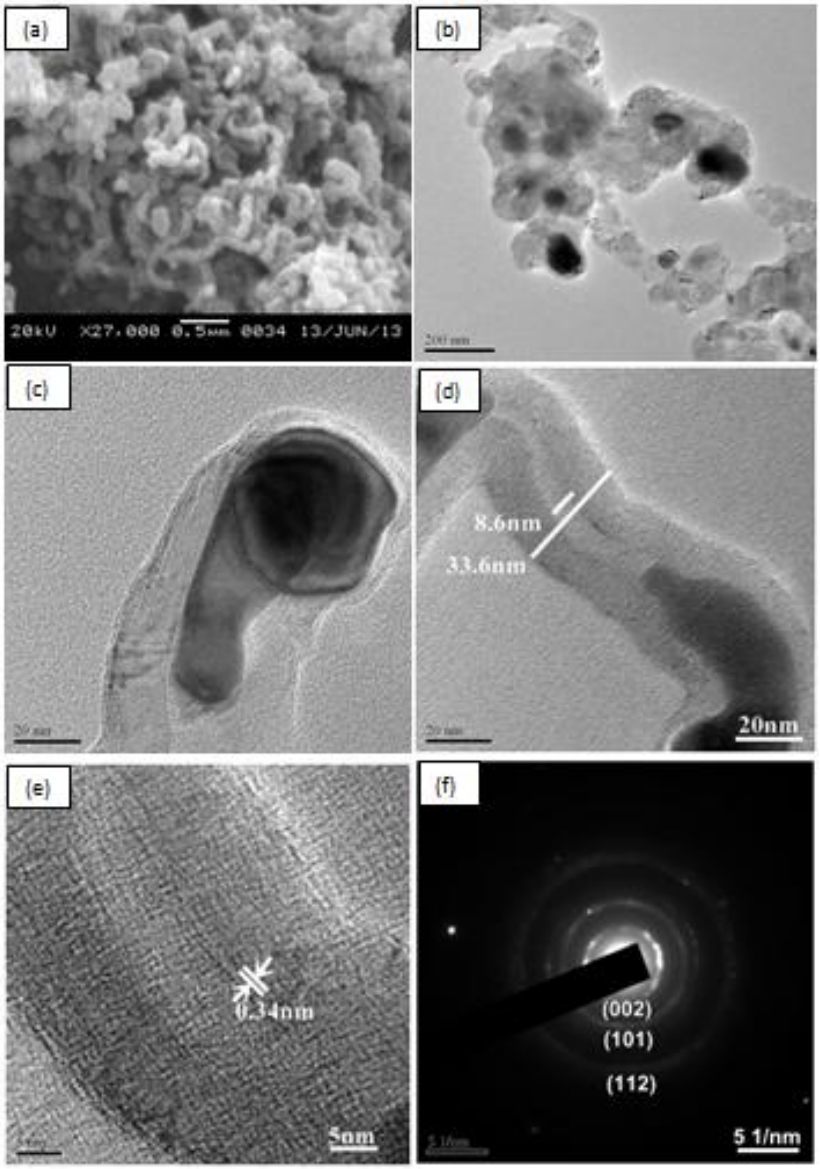

Fig.3.22. (a) SEM micrograph **(b-d)**TEM micrographs **(e)** HRTEM micrograph**(f)** SAED patternof MWCNT obtained from sunflower oil using catalyst

3.6.3.2 XRD analysis of MWCNT from sunflower oil

Both graphitic carbon and face centered cubic nickel phase were observed in the XRD pattern**(Fig.3.23).**The X-ray diffraction pattern showed sharp and intense peaks at 44.75^0 and 52.21^0which correspond to the (111) and (200) crystallographic planes of fcc Ni (JCPDS file no.04-0850) and peaks at 2θ values26.62^0, 44.58^0 and 51.87^0 correspond to the (002), (101) and (102) crystallographic planes of hexagonal graphitic carbon (JCPDS file no. 23-0064). The interlayer spacing (d_{002} =0.33nm)

using Bragg's formula, nλ=2dsinθ, similar to that of graphite (0.33nm), shows orderly stacking in the MWCNT. The average crystallite size estimated by the Debye-Scherrer equation using a Gaussian fit was found to be 10.4 nm for (002) plane of graphite.

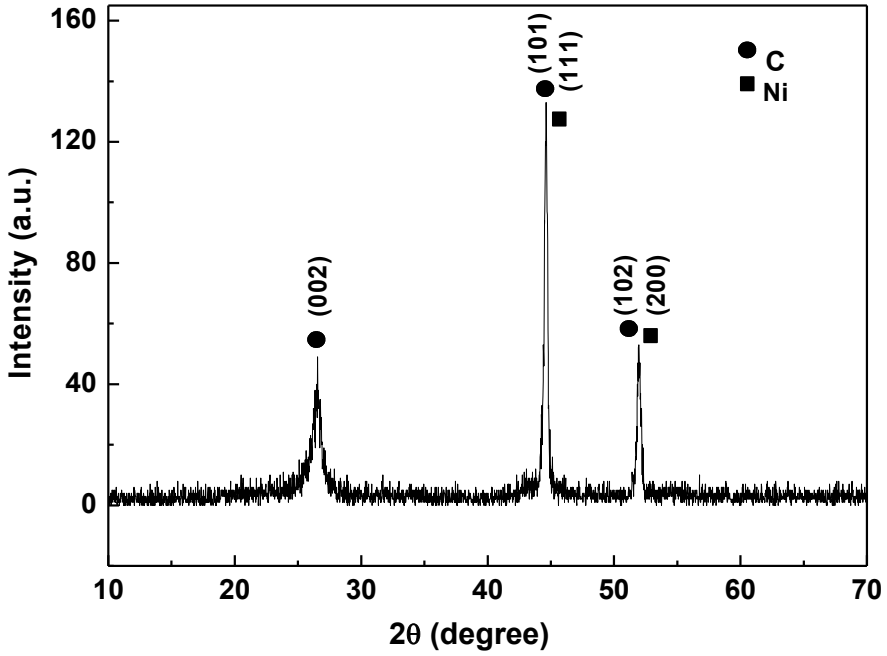

Fig.3.23. XRD pattern of MWCNT from sunflower oil using catalyst

3.6.3.3. Antioxidant activity of MWCNT from sunflower oil

The antioxidant activity of as obtained MWCNT synthesised from sunflower oil was measured based on the scavenging abiliity of the stable 2, 2-diphenyl 2-picrylhydrazyl (DPPH) free radical (*vide supra*insection**3.4.3.5.** of this chapter)[111,124]. The DPPH scavenging percentage were calculated from decline in absorbance at 517 nm, which corresponds to the quantity of DPPH in methanolic solution. It is evident from the **Fig.3.24 (b)** that after 30 minutes more than50% of the DPPH got scavenged for 6 mg of the MWCNT. The SC-50 value was ascertained graphically (**Fig.3.24 (f))** and was foundto be 5.57 mg. A similar mechanism can be predicted for the antioxidant behaviour of CNT as described insection**3.4.3.5**of this chapter (**Fig. 3.14).**

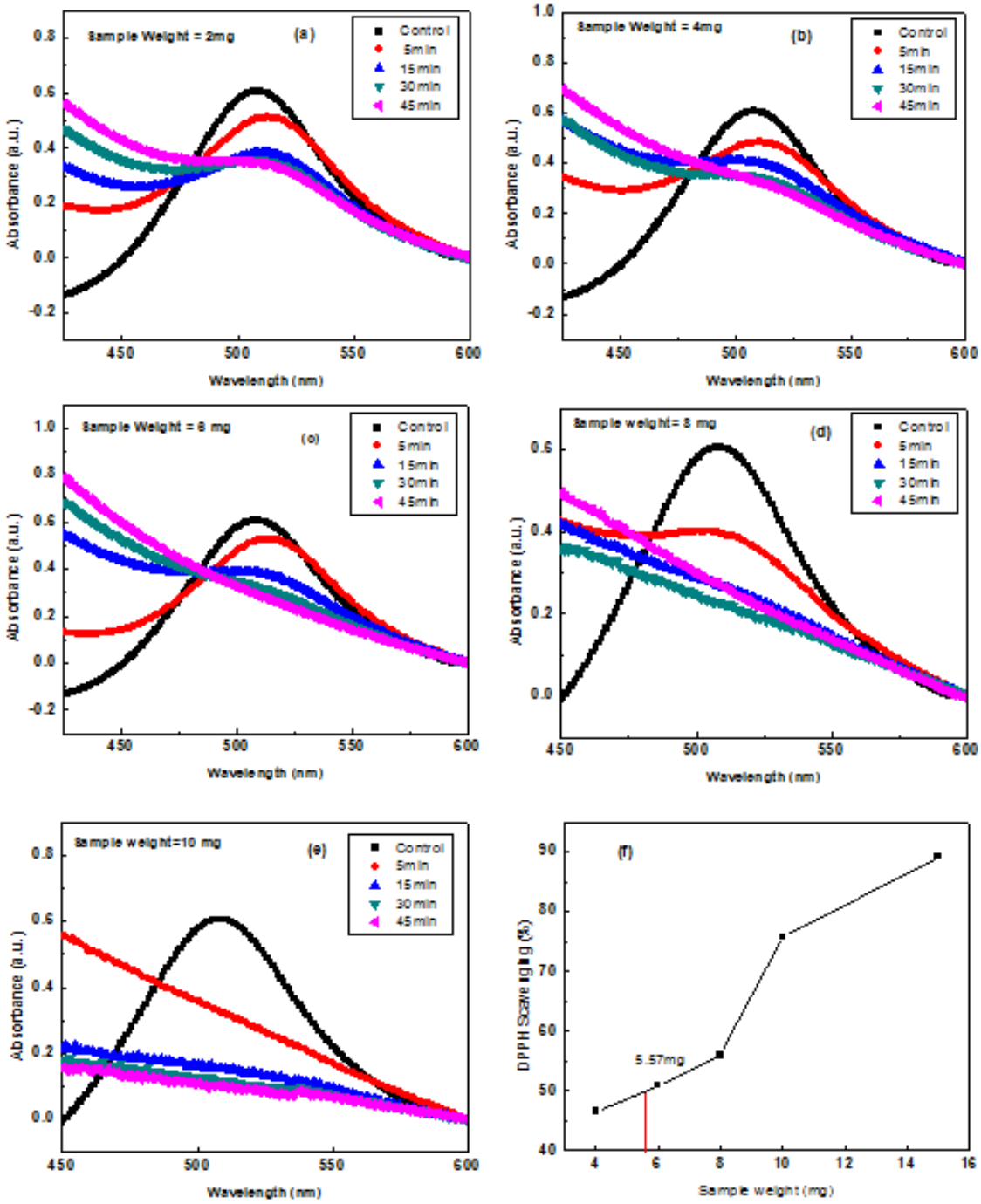

Fig.3.24. (a-e) Time dependent DPPH scavenging by varying MWCNT concentration**(f)** DPPH scavenging (%) at different weight of MWCNT

3.7. Multiwalled carbon nanotube from refined mustard oil

3.7.1. Materials

Refined mustard oil is used as carbon source for the synthesis of MWCNT. Mustard oil derived from mustard seeds. The characteristic pungent flavour of mustard oil is due to allyl isothiocyanate. Mustard oil has about 60% monounsaturated fatty

acids(42% erucic acid and 12% oleic acid), it has about 21% polyunsaturated fats (6% the omega-3 alpha-linolenic acid and 15% the omega-6linoleic acid) and it has about 12% saturated fats.

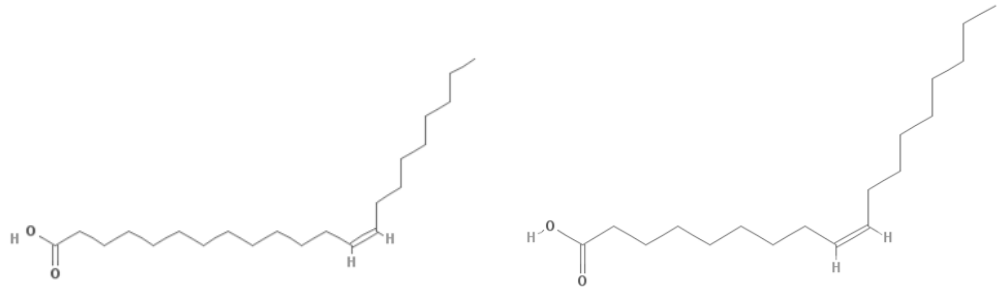

Erucic acid Oleic acid

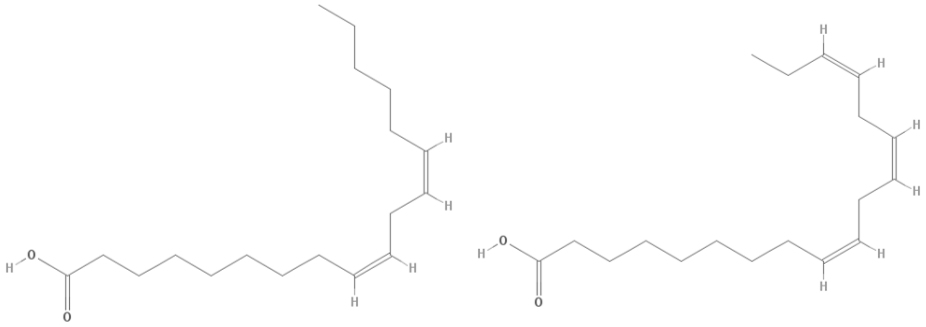

Linoleic acid Linolenic acid

Fig.3.25. Chemical structure of major components of carbon source: mustard oil

3.7.2.Synthesis of MWCNT from refined mustard oil

The MWCNTs were prepared by CVD method from refined mustard oil using nickel nanoparticles as catalyst. The synthetic procedure is similar to that mentioned in the section **3.3.2.** of this chapter. The furnace temperature was750°C and constant argon atmosphere was maintained. In order to remove the catalyst particles, the as obtained black powder were treated with dilute acid (6M HCl) followed by washing with deionised water. The yield recorded was~2.9 g.

3.7.3. Results and discussion

The as obtained black powderwas found to be stable in air for months and can be dispersed in aqueous and organic solvents (methanol, ethanol) under ultrasonication. The yield of the material was recorded to be around 29% of initial mass. Tap density of the material was calculated to be 0.45gcm^{-3}. Although CNTs were efficiently synthesized without using any external catalysts from turpentine oil, sesame oil etc.,

however, the catalyst free CVD synthesis from refined mustard oil at varying temperatures afforded glassy carbon, diamond like carbon (DLC) and agglomerated products only.

3.7.3.1.Scanning electron microscopy and transmission electron microscopy

The SEM micrograph (**Fig.3.26 (a,b)**) revealed the presence of bundles of non-uniform nanotubes. The TEM micrographs (**Fig.3.26(c,d)**) revealed bundles of hollow multiwalled carbon nanotubes.As can be seen from the figures, the as-grown CNTs are clean and metal and other carbonaceous materials are significantly less.These CNTs have an empty and uniform central core with one end open.

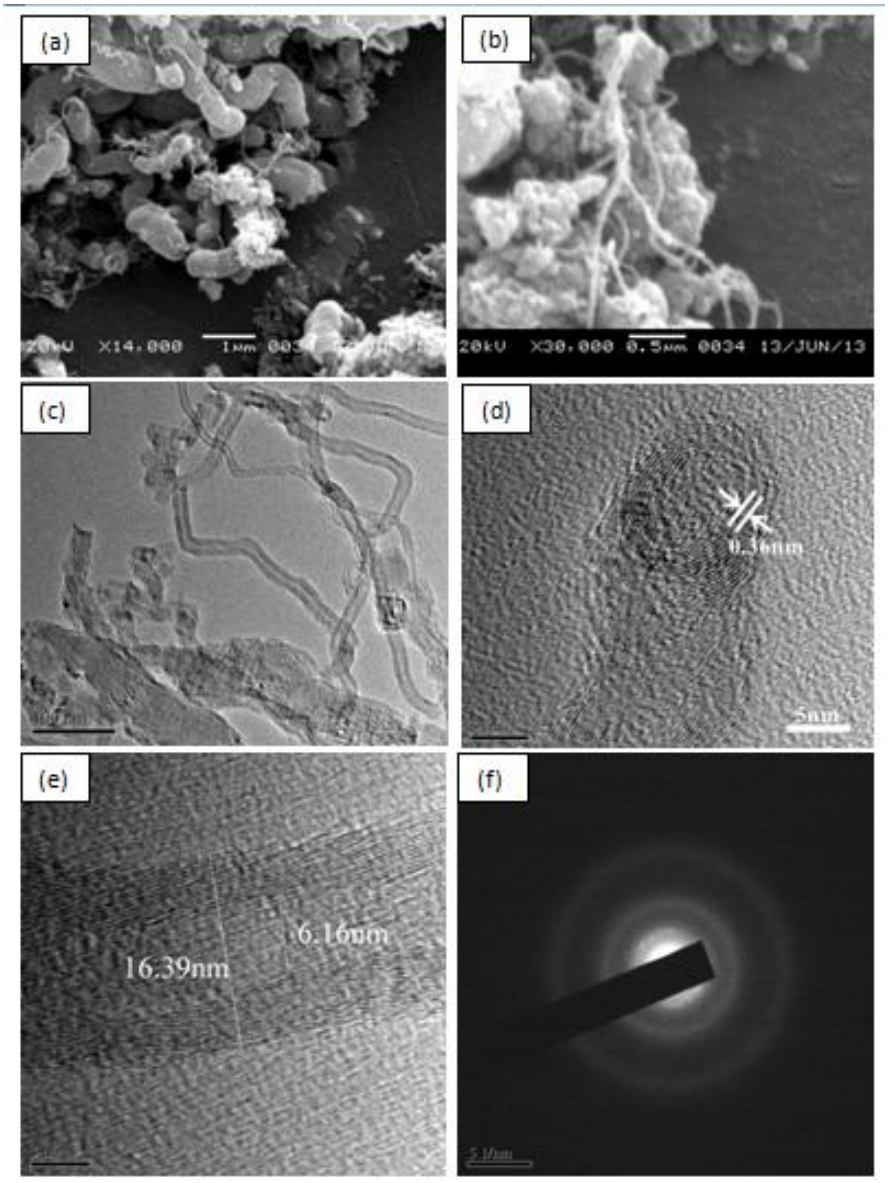

Fig.3.26. (a,b) SEM micrographs **(c)** TEM micrograph **(d,e)** HRTEM micrographs**(f)** SAED patternof MWCNT obtained from refined mustard oil using catalyst

3.7.3.2. X- ray diffraction analysis of MWCNT from refined mustard oil

The powder X-ray diffraction pattern was recorded for identification of phases exhibited by the synthesised material.**Fig.3.27**exhibited a number of intense and sharp peaks assigned toBragg reflections from both carbon and nickel. The peaks at 2θ values 26.79^0, 42.72^0, 44.75^0, 50.35^0 and 54.42^0 correspond to the (002), (100), (101), (102) and (004) crystallographic planes of hexagonal graphitic carbon (JCPDS file no.23-0064) and peaks at 44.92^0 and 52.04^0 correspond to the (111) and (200) crystallographic planes of face centered cubicnickel (JCPDS file no.04-0850).The interlayer spacing (d_{002}= 0.34nm) found from XRD was characteristic of graphitic carbon.The average crystallite size estimated by the Debye-Scherrer equation using a Gaussian fit was found to be 8.5 nm for 002 plane of graphite.

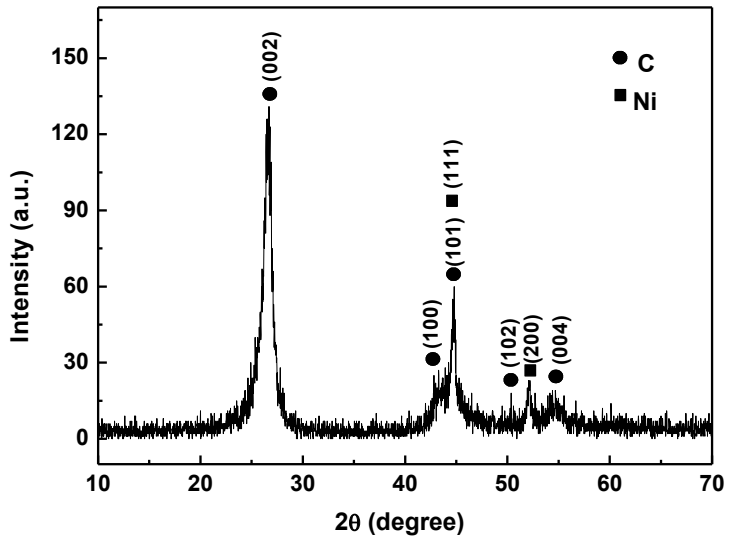

Fig.3.27. XRD pattern of MWCNT obtained from mustard oil using catalyst

The specific surface area (S) calculated by Sauter formula, S=6000/ρ×D, where D is the crystallite size and ρ is the density of the synthesized material [116,117], and was found to be 1410 m^2/g.

3.7.3.3. Electrochemical behaviour of MWCNT from refined mustard oil

The electrochemical behaviour of MWCNT was monitored by using both cyclic voltammetry (CV) and constant current or galvanostatic charge/discharge method. It would be useful at this point to furnish in the following section, a brief account pertaining to the theoretical background and experimental approaches currently in

vogue for studying cyclic voltammetry, charge/discharge of materials. The results obtained in the present research are discussed thereafter.

Relevant equations/mathematical relations for calculations of Capacitance and Specific capacitance are appended below:

$$C = I \times dt / dv$$

Where, C: capacitance, F

I: current which goes to the capacitor, A

t: charge or discharge time, second

v: voltage difference between two electrodes, V

Capacitance for cyclic voltammetry,

$$c_{total} = \frac{I}{s}$$

Where C_{total}= capacitance of total electrode, F

I= current, A

s= scan rate, V/s

$$Csp = \frac{I}{s \times W}$$

Where, Csp= total specific capacitance of cell, F/g

W = total weight of the material used for construction of cell, g

For a capacitor with two electrodes, the total capacitance is C_{total}.

$$1/C_{total} = 1/C_{cathode} + 1/ C_{anode}$$

Where, $C_{cathode}$is capacitance for cathode electrode, F

$C_{anode}$is capacitance for anode electrode, F

For a symmetrical cell, $C_{cathode} = C_{anode} = C_{single}$

$$C_{total} = C_{single}/2 \text{ or } C_{single} = 2 \text{ x } C_{total}$$

Where, C_{single} is capacitance of single electrode, F. Thus, for a double electrode capacitor, the value of capacitance of a single electrode is two times the total capacitance measured.Specific capacitance of a single electrode in a capacitor cell is calculated using this formula,

$$C_P = \frac{2 \times I}{\frac{dv}{dt} \times w} = \frac{2 \times C_{total}}{w}$$

Where, C_P: specific capacitance of single electrode, F/g

w: active material mass on single electrode, g

I: current which goes to the capacitor, A

t: charge or discharge time, second

v: voltage difference between two electrodes, excluding the portion of ohmic drop, volts

3.7.3.3.1. Cyclic Voltammetry

Cyclic voltammetry is the most frequently used and often the first measurement executed for understanding an electrochemical system. Itis performed within a predetermined potential range to avoid gas revolution and at a fixed scan rate, i.e. a linear variation of potential with time. The resulting Potential (E)-Current (I) plot i.e., forward and backward scans is named a cyclic voltammogram where current is a response on Y-axis and potential on X- axis (**Fig.3.28 (A)**). As shown in**Fig.3.28 (A)**, a rectangular cyclic voltammogram suggests a pure capacitive behavior of an ideal double layer capacitor without any chemical reaction. Graph (X) shows absence of an electrochemical reaction in the selected potential window. Difference between the anodic current and cathodic current i.e., charging current is considered as the total current available by the capacitor. An absence of typical rectangular voltammogram in the graph (Y) indicates presence of some electrochemical reaction. Thus material used in graph X is useful for the fabrication of supercapacitor. **Fig. 3.28(B)** is a cyclic voltammogram of a system with reversible redox reaction or Faradic reaction.

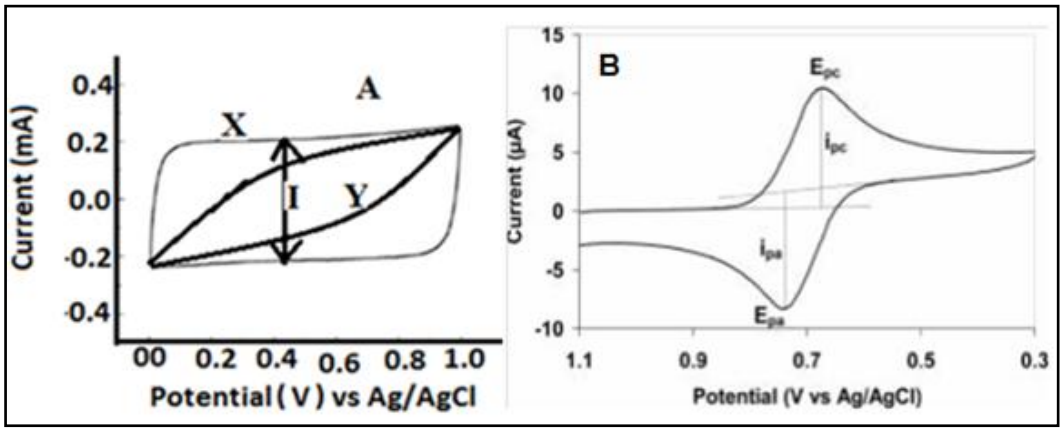

Fig.3.28. (A) Cyclic voltammogram of double layer capacitor; a rectangular graph (X) confirming no electrochemical reactions in potential range of 0.0 V to 1.0 V while graph (Y) did not show any constant current in the selected potential range**(B)** pseudo capacitor showing typical oxidation and reduction peaks [118]

[*Source*:Xu, B., Wu, F., Chen, R., Cao, G., Chen, S., Wang, G., & Yang, Y. *J. Power Sources*, 2006, **158**, 773]

In the present work, a two-electrode system has been used to evaluate the performance of capacitor cell in 1N KOH electrolyte. The cyclic voltammogram of synthesised material at scan rates of 5 to 500 mV/s exhibited capacitive behaviour with respect to applied voltage of -0.4 to 0.4 V (**Fig.3.29(a)**). CV curve showed a quite rectangular shape at 5 mV/s indicating well developed capacitance properties. Up to the scan rate of 200mV/s, the CV curve shows rectangular shape after that it shows elliptical behavior.

Table 3.1 Specific capacitance at different scan rate

Scan rate (mV/s)	Current (mA)	Total specific capacitance(F/g)	Specific capacitance of a single electrode (F/g)
5	0.49	49.99	99.98
10	0.74	37.17	74.34
20	1.64	31.20	62.40
50	2.41	24.16	48.32
100	4.19	20.97	41.94
200	6.66	16.66	33.32
500	12.21	12.21	24.42

It is observed that scan rate is inversely proportional to specific capacitance(**Table 3.1**). As the scan rate increases, current increases but specific capacitance decreases (**Fig.3.29 (b)**). It is believed that slowing down the scan rate can allow electrolyte to penetrate into pores more thoroughly and to make greater contact with the internal surface of the electrode material and hence more charge is stored on the surface of electrode and yield a larger measured capacitance that is closer to the intrinsic capacitance. Whereas at higher scan rate electrolyte get less time to contact with the complete electrode surface and less charge stored on electrode surface which result into low capacitance [119, 120].

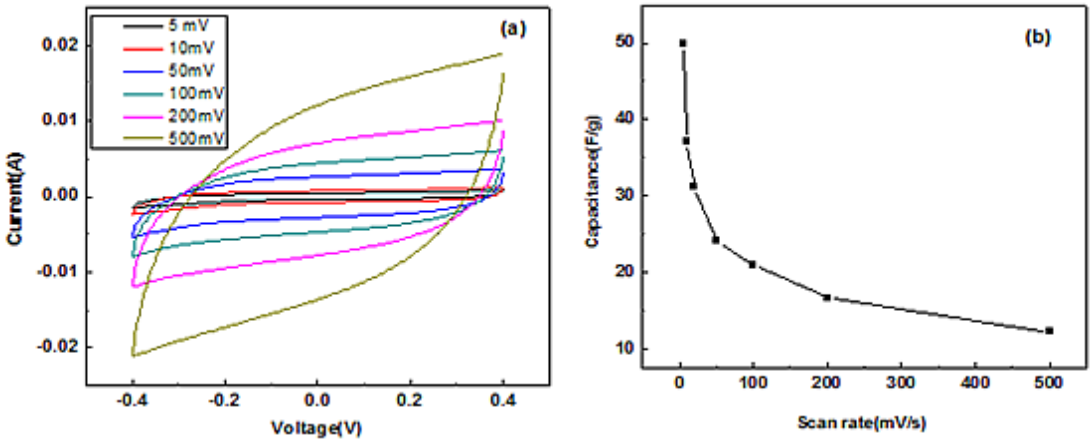

Fig.3.29. (a) CV curve of as-obtained MWCNT at different scan rate (5 - 500 mV/s)in1N KOH solution **(b)**Effect of scan rate on capacitance

3.7.3.3.2. Constant current or galvanostatic charge/discharge(CD)

Constant current or galvanostatic charge/discharge is in principle the same technique as cyclic voltammetry but with fixed current and charge/discharge time. Thus, the potential is obtained as a response on Y-axis and slope of CD curve represents the scan rate.

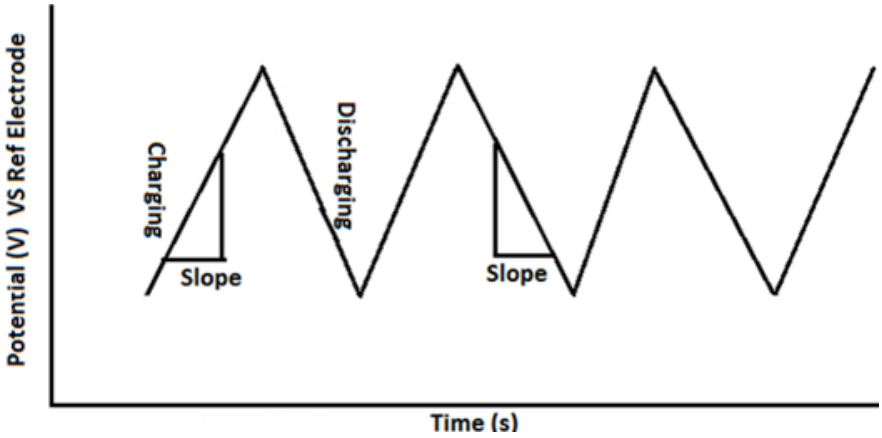

Fig.3.30. Five cycles of constant current charge/discharge

In the present work, constant current or galvanostatic charge/dischargewas also used to evaluate the capacitance of the synthesised material. **Fig.3.31** showed the graph of Charge-Discharge cycle where the slope of the CD curves represents the scan rate of around 10mV/s. During the test, 1mA was used as the constant current, consistent with the CV measurement. The potential range was kept between -0.4 to 0.4V. It is found that the charge curves are very symmetric to their corresponding discharge

counterparts in the potential range. The symmetry of the charge and discharge characteristics shows good capacitive behavior suggestive of a good charge storage performance.

The specific capacitance of the synthesised sample determined using the CD method at 10mV/s was 33.22 F/g that was slightly lower than that obtained with the CV method (37.17 F/g). This may be attributed to the fact that when calculating capacitance from the CD curve, the voltage drop (also called IR drop) at the change of charge to discharge indicates internal resistance is excluded from the rest of the curve, but the calculation of the CV based capacity uses the entire curve that includes the IR effect.

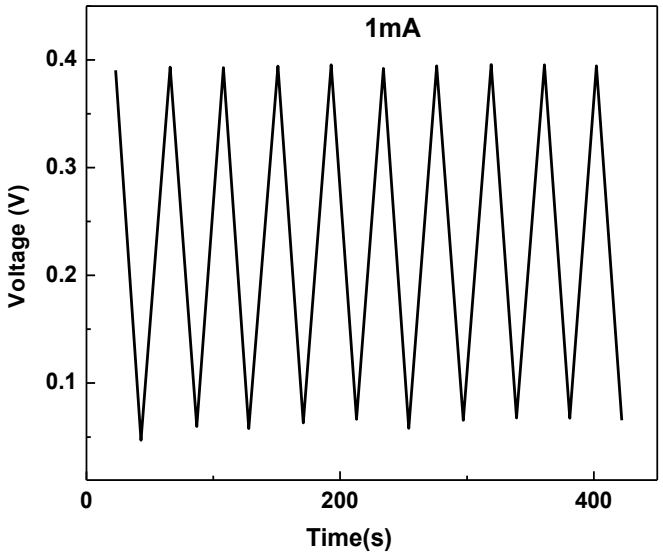

Fig.3.31. Charge-discharge curves of a capacitor cell made with as-obtained MWCNT at current of 1mA

3.8. Multi walled carbon nanotubes (MWCNT) from *ghee* (clarified butter from cow's milk)

3.8.1.Materials

Clarified butter more commonly called *ghee* in India is pure butterfat left over after the milk solids and water are removed from butter (**Fig.3.32**). It is used widely in Indian cooking. Like clarified butter, *ghee* is made by melting butter, cooking off the water and separating the clear, golden butter fat from the milk solids. Unlike commercially available butter, *ghee* in Indian tradition is simmered for a little while, thus browning the milk solids and adding a slightly nutty flavour to the finished

product. Not all *ghee* recipes necessarily specify the browning of the milk solids, however, for all practical purposes *ghee* is clarified butter.

Ghee is better for high-heat cooking than butter since it has a smoke point of ~ 240°C compared to 175°C for ordinary butter. Another advantage of *ghee* is that it has a longer shelf life and when stored in an airtight container can be preserved at room temperature for years. The *ghee* used in the present work is obtained from cow's milk using traditional Indian procedure (vide infra).

Fig.3.32. *Ghee* (clarified butter from cow's milk)

3.8.2. Synthesis of MWCNT

The MWCNTs were prepared by CVD method from *ghee* without using any catalyst. A quartz boat loaded with fresh ghee (10 g) was kept in a lower-temperature zone (300^0C) and an empty quartz boat was kept at a higher temperature zone (750^0C) in a horizontal quartz tube. Hydrogen gas was then purged at a rate of $6cm^3$/min. The furnace was heated to 750^0C at a rate of 7^0C /min for 2 hours and then allowed to cool to ambient temperature whereupon the CNTs were obtained as black powder (yield ~3.6 g).

3.8.3. Results and discussion

The 'as obtained'material wasblack and amorphous in appearance, found to be stable in air for months, and can be brought into dispersion in both aqueous and organic solvents by ultra-sonication. The yield of the product was found to be 36% of the initial weight. The tap density of the MWCNTs was calculated to be about 0.61 g/cm^3.

3.8.3.1. Scanning electron microscopy and transmission electron microscopy

The SEM micrograph (**Fig.3.33**) revealed the presence of intertwined bundles of micrometer length CNTs.

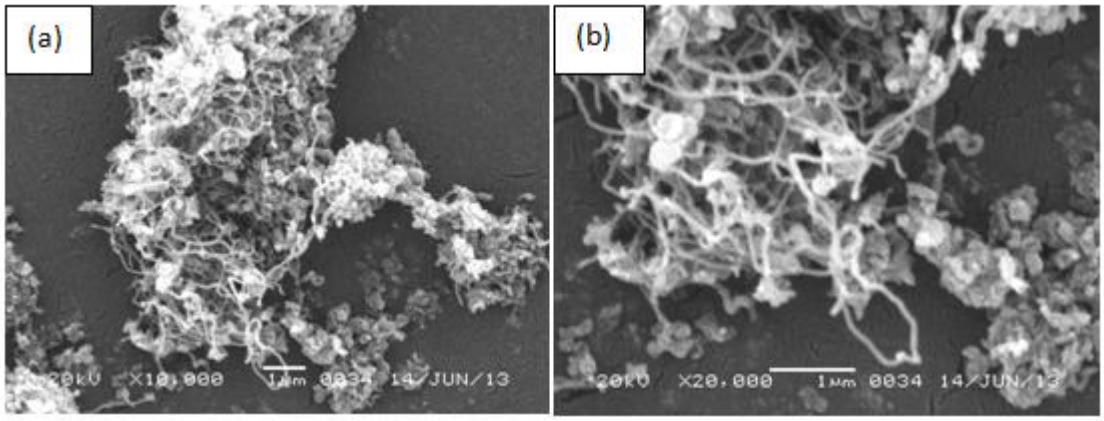

Fig.3.33. (a, b)SEM micrographs of as-obtained CNT from *ghee*

The TEM micrographs (**Fig. 3.34(a,b)**) revealed the tubular structure of nanotubes. The HRTEM image (**Fig.3.34(c)**) suggested that the as-grown nanotubeshave an empty and uniform central coreand consisting of concentrically nested ~ 25 graphene cylinders with the outer and inner diameters 27.45 and 13.68 nm, respectively. The interlayer distance is about 0.33 nm which resembles that of (002) plane of the standard graphitic carbon.

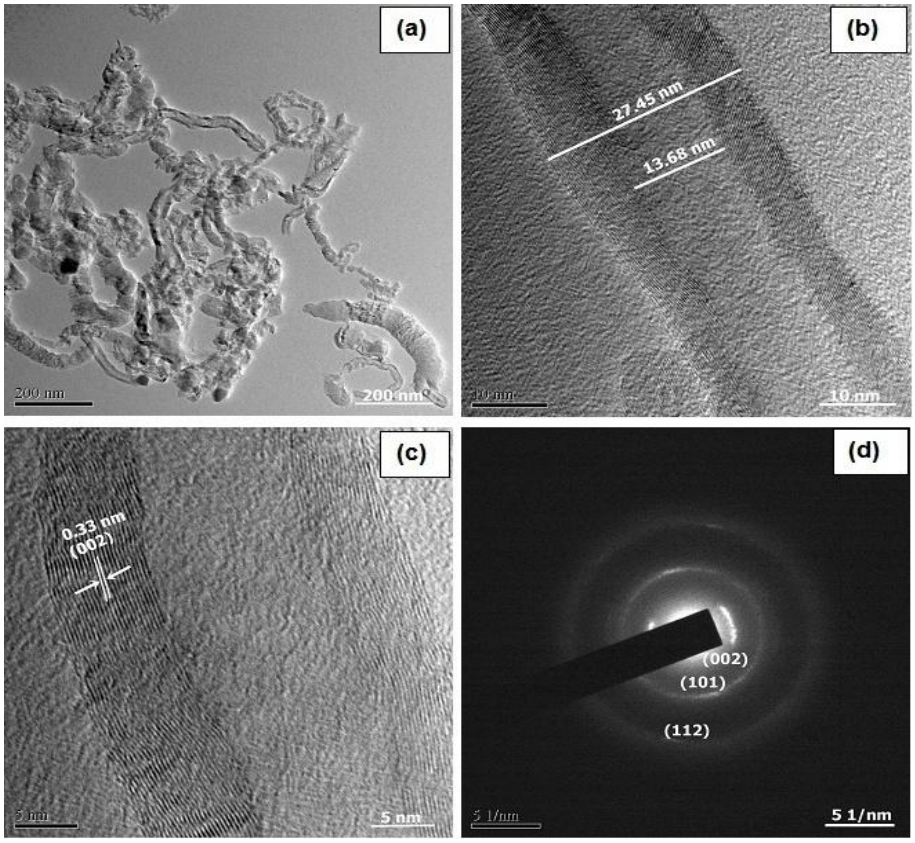

Fig. 3.34. (a,b) TEM micrographs **(c)** HRTEMmicrograph **(d)** SAED pattern of MWCNT from *ghee*

The SAED pattern showed the concentric rings indicating polycrystalline nature of the material (**Fig.3.34(d)**). Undesirable structures like amorphous carbon are negligible suggesting that the as synthesized MWCNTs are reasonably purewhich is also concordant with XRD data.

3.8.3.2. X-ray diffraction study of MWCNT from *ghee*

The powder XRD pattern of the synthesized MWCNT is shown in (**Fig. (3.35**). A number of strong Bragg reflections were obtained in the pattern corresponding to the (002), (100), (101) (102) and (004) reflections of hexagonal graphitic carbon (JCPDS Card No. 23-0064 possessing space group $P6_3/mmc$). The presence of (002) peak in the XRD spectrum indicates that the concentric cylindrical nature of graphene sheet (d_{002} = 0.34nm) nested together, and the nanotubes were multiwalled in nature. The interlayer spacing (d_{002} = 0.34nm) found by XRD is consistent with that obtained (d_{002} ~ 0.33 nm) from HRTEM and is characteristic of CNTs. The average crystallite size estimated by the Debye-Scherrer equation, $d=0.9\lambda/\beta\cos\theta$ using a Gaussian fit was found to be 4.6 nm.

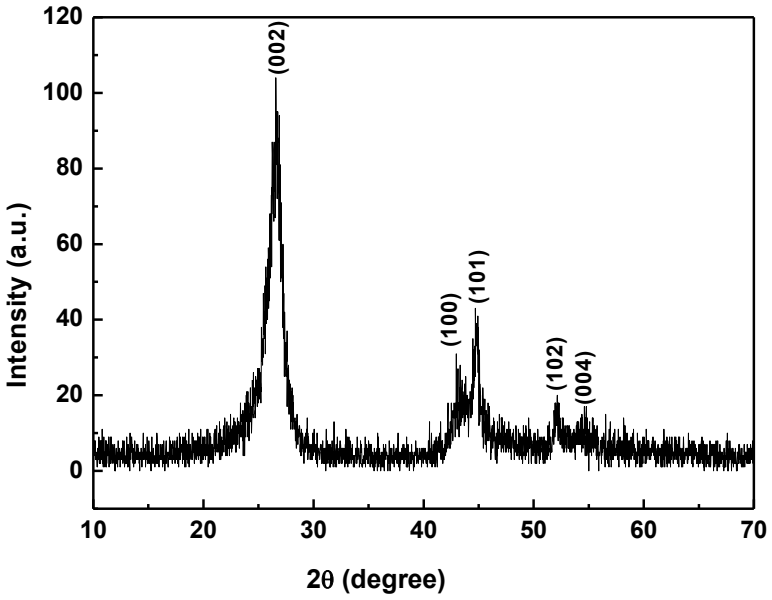

Fig.3.35. XRD pattern of the as obtained MWCNTfrom *ghee*

The average crystallite size and lattice strain estimated using Williamson-Hall equation, $\beta\cos\theta = k\lambda/d + 4\varepsilon\sin\theta$, for all peaks from $2\theta = 10^0$ to $2\theta = 70^0$ [121-123]. The average crystallite size and the strain were determined to be 20.6 nm and

2.083×10^{-3} respectively. The average crystallite size calculated by the Debye-Scherrer equation is lower than that obtained from Williamson-Hall plot. This difference is attributed to the strain induced nanocrystal defects.

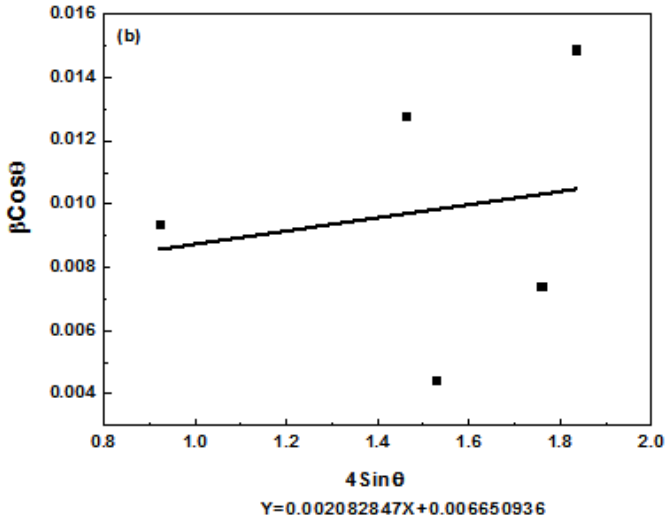

Fig.3.36. Williamson-Hall plot ofMWCNT from ghee

The specific surface area (S) calculated by Sauter formula, S=6000/ρ×D, where D is the diameter and ρ is the density of the synthesized material [116,117] and was found to be 477.0 m^2/g.

3.8.3.3. Antioxidant activity of MWCNT from *Ghee*

The antioxidant activity of the MWCNTs was studied in an *in vitro* system, using modified DPPH method as reported bySerpen *et. al* [111] for insoluble solid materials.The DPPH reducing ability of MWCNTs was assessed spectrophotometrically by observing color change from purple to yellow[124]. The UV-visible absorption of DPPH is invariant of time. MWCNTs with DPPH added, however, showed a steady decrease in absorbance at517 nm (**Fig.3.37**). The DPPH scavenging percentage thus calculated corresponds to the quantity of DPPH in the methanolic solution. As evident from (**Fig.3.37(a-e)**), more than 50% and 70% of the DPPH were scavenged after 30 min and 60 min, respectively for 4 mg of the as-prepared MWCNTs. The SC50 value was ascertained graphically (**Fig.3.37(f)**) to be 3.8 mg.

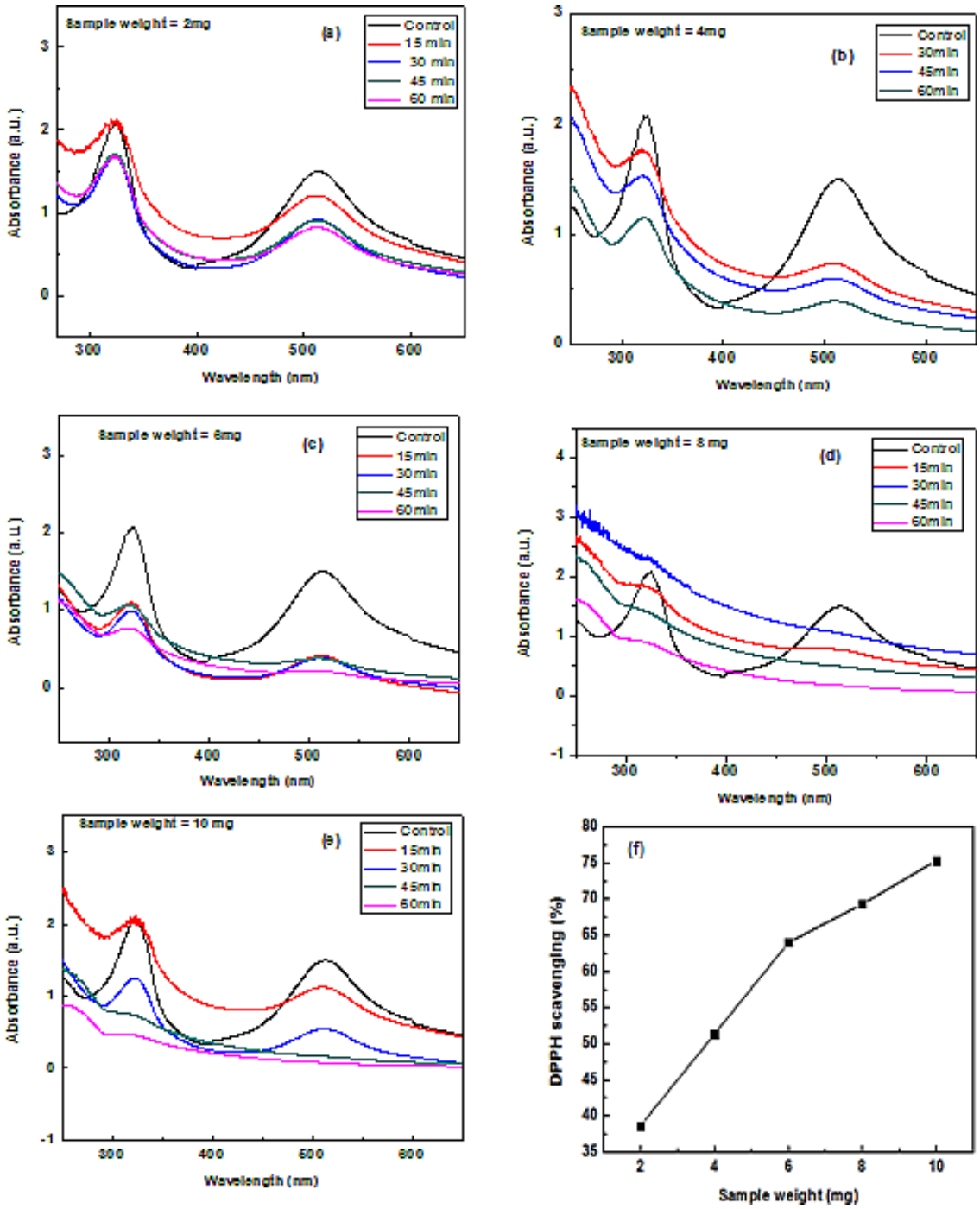

Fig.3.37. (a-e) Time dependent DPPH scavenging by varying MWCNT concentration**(f)** DPPH scavenging (%) at different weight of MWCNT

In drawing a correlation of this result with those obtained for seasame oil and sunflower oil (*vide supra* in this chapter) an interesting pattern that emerges is that the scavenging efficiency could be correlated to average particle size of the CNTs obtained by Debye-Scherrer calculations. A higher crystallite size tend to lower the efficacy of the material towards the free radical scavenging.

Table 3.2 Antioxidant efficacy of MWCNTs

MWCNT	Average crystallite size	SC-50
From Ghee	4.60 nm	3.80 mg
From sesame oil	7.53 nm	4.83 mg
From Sunflower oil	10.42 nm	5.57 mg

3.9. Carbon nanowhiskers / nanonecklace and carbon nanorings from palmolein oil using nickel nanoparticle as catalyst

3.9.1. Materials

Palmolein oil is used for the synthesis of carbon nanowhiskers /nanonecklace and Carbon nanorings.Palmoleinis the main products frompalm trees (*Elaeis guineesis*). Palmolein oilis composed of fatty acids, esterifies with glycerol. It oil has an especially high concentration of saturated fat, specifically, of the 14-carbon saturated fatty acid palmitic acid, to which it gives its name. Monounsaturated oleic acid is also a major constituent of palmolein oil.

3.9.2. Synthesis of carbon nanowhiskers / nanonecklace and carbon nanorings

The carbon nanowhiskers/ necklace and carbon nanorings were prepared by CVD method in two separate experiments from palmolein oil using nickel nanoparticles as catalyst by varying the CVDtemperature.

General procedure:

A quartz boat loaded with palmolein oil (~10 g) was kept in a lower-temperature zone (300°C) and another quartz boat in which 1mg of nickel nanoparticles previously dispersed uniformly using ethanol was kept at a higher temperature zone (750°Cfor nanowhisker / necklace and 650^0C for nano rings) in a 1m long horizontal quartz tube in the CVD furnace. Argon gas was then purged at a rate of $6cm^3$/min. The furnace temperature was maintained separately at two different temperatures 750^0C and 650^0C for 2 hoursand then allowed to cool to ambient temperature whereupon the respective products were obtained. The catalyst particles were removed by washing with mild

acid solution in order to retain the inherent morphology. The yieldwas recorded to be ~2.4 g and ~2.6g, respectively.

3.9.3. Results and discussion

The as obtained black powderswere found to be air stable and can be dispersed in aqueous and organic solvents under ultrasonication. The temperature and catalyst plays a crucial role in the synthesis of whisker and ring as at higher temperature whiskers were formed while lower temperature favoured nanorings. Temperature below 650^0C yielded agglomerated product. The catalyst free chemical vapour deposition of palmolein oil yielded glassy carbon only. It would be relevant herein to mention that at a temperature of 950^0C carbon micro and nanospheres [125] and carbon nanotubes [126] were produced from palmolein oil.Carbon nanohorn-multi walled carbon nanotube hybridswere accessed by chemical vapour deposition method at 950^0C was from bio-renewable resource palmolein. Such carbon nanostructures are useful forvarious applications from electronics to medical applications. This is ascribed to theirsuperior properties *vis-a-vis* their bulk counterpart. Carbon nanohorn due to their unique microporous structures and a high surface area possess potential for gas storage, biosensing,drug delivery and catalyst support.

3.9.3.1. Scanning electron microscopy andtransmission electron microscopy of carbon nanowhisker/nanonecklace

The SEM micrographs (**Fig.3.38 (a)**) of the as-obtained material from palmolein oil using nickel nanoparticle catalystby CVD at750^0C revealed bundles of nanowhiskers. The TEM micrographs (**Fig.3.38 (b,c)**) indicated the presence of micrometer long necklace or whiskers. The HRTEM image (**Fig.3.38 (d, e)**) showed that the as-grown whiskers seem to arrange in the form of a necklace and the lattice fringes between two adjacent planes are 0.34nm apart, which corresponds to the interlayer separation of (002) plane of the graphitic carbon. The SAED (**Fig.3.38(f)**) revealed concentric rings that are characteristic of graphitic carbon.

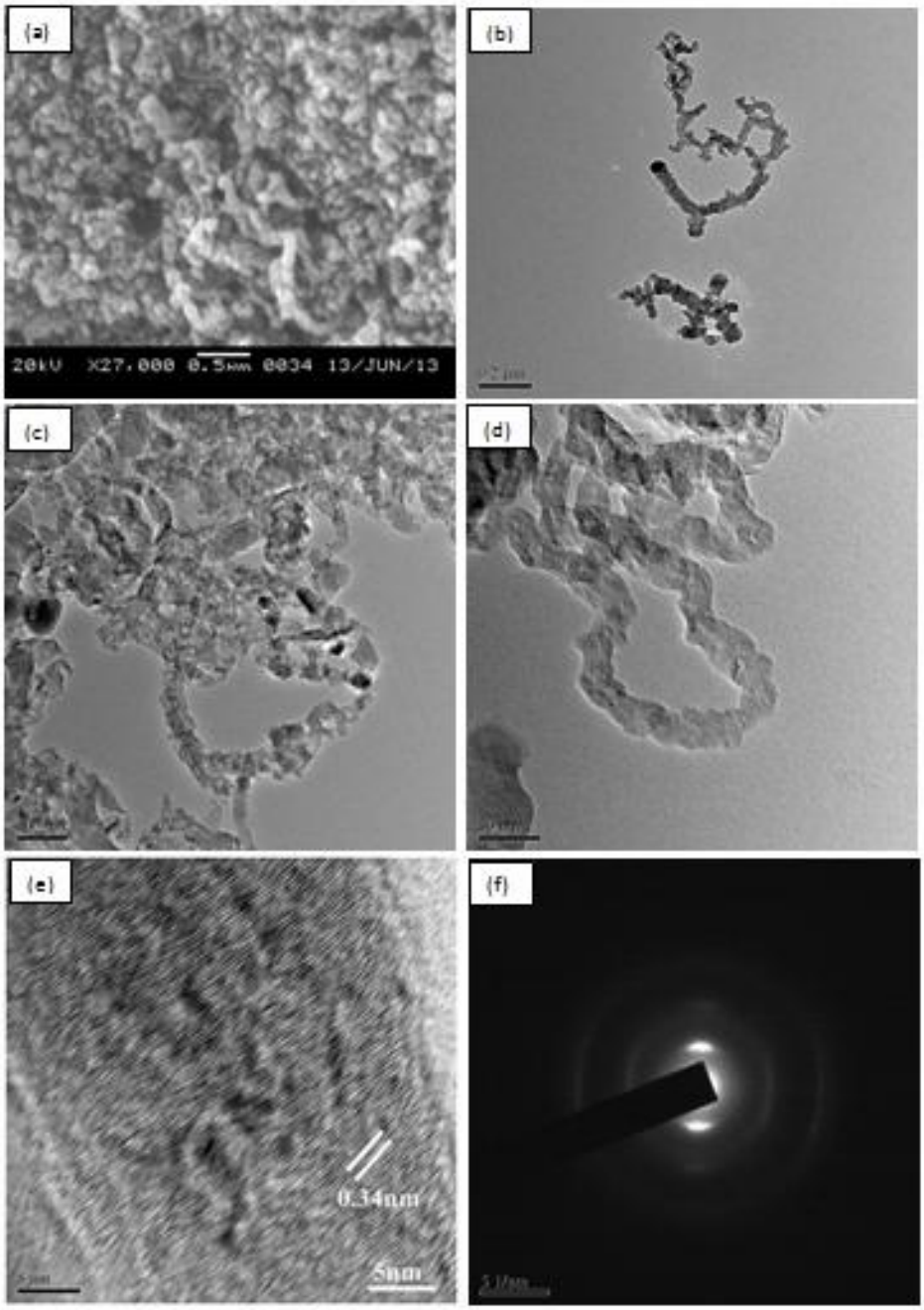

Fig.3.38. (a)SEM micrograph **(b,c)** TEM micrographs **(d,e)** HRTEMmicrograph**(f)** ED pattern of nanowhisker/necklace

3.9.3.2. Transmission electron microscopy of carbon nanorings from palmolein oil

The TEM micrographs (**Fig.3.39. (a-d)**) indicated the presence of graphitized carbon nanorings with ~65 layers of graphene sheets. The dark portion inside ring might be attributed to the presence of catalyst particles. From HRTEM image (**Fig.3.39(e)**) lattice fringes were observed having interlayer distance 0.34 nm which resembles that

of (002) plane of graphitic carbon. The SAED pattern(**Fig.3.39(f)**) revealed concentric rings along with spots. The rings are characteristic of graphitic carbon while spots could be attested to nickel nanoparticle catalyst.

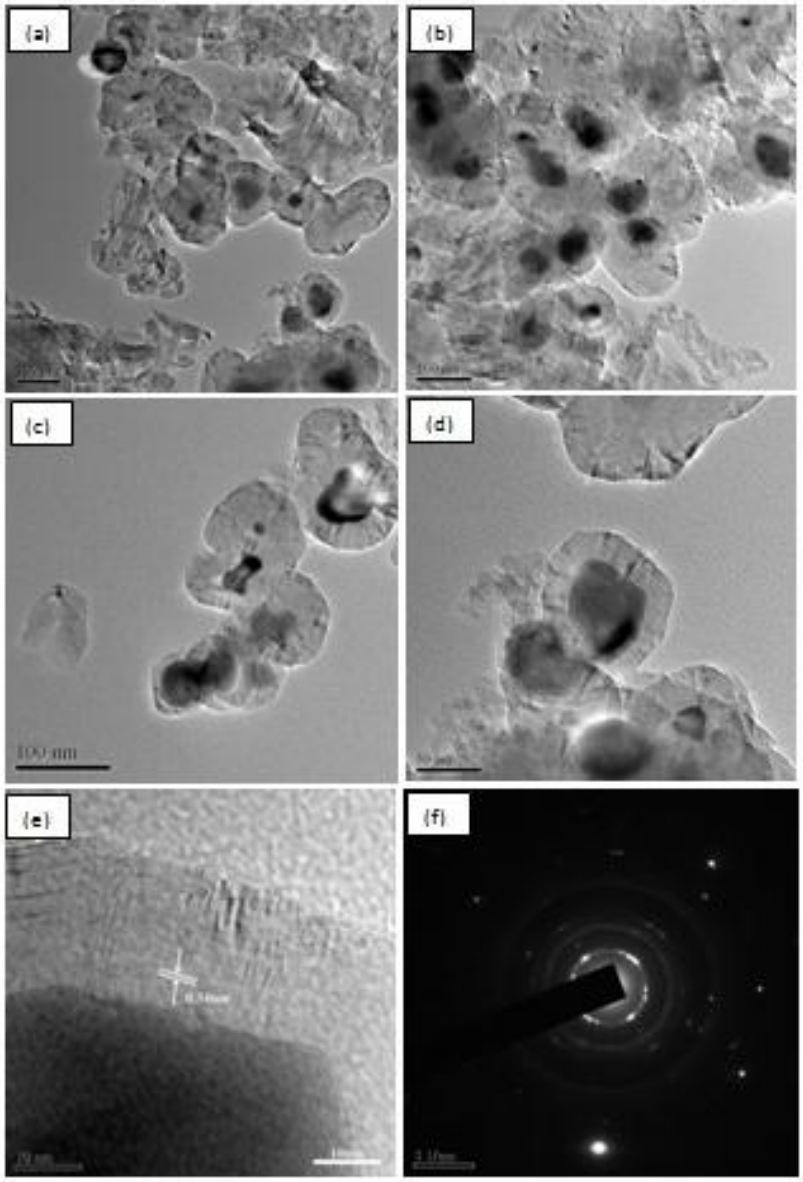

Fig.3.39. (a-d) TEM micrographs **(e)** HRTEM micrograph**(f)** SAED pattern of carbon nanorings from palmolein oil

3.9.3.3. XRD pattern of carbon nanowhiskers and carbon nanorings

The XRD pattern **(Fig.3.40(a))** of CNW and that of carbon nanorings **(Fig.3.40(b))** obtained frompalmolein oilexhibited sharp peaks of carbon and nickel. The pattern in both the cases exhibited peaks of characteristic graphitic plane and face centered cubic nickel crystallographic plane. The average crystallite size estimated by the

Debye-Scherrer equation for carbon nanowhiskers was found to be 7.6 nm and that for nanorings was 8.2 nm.

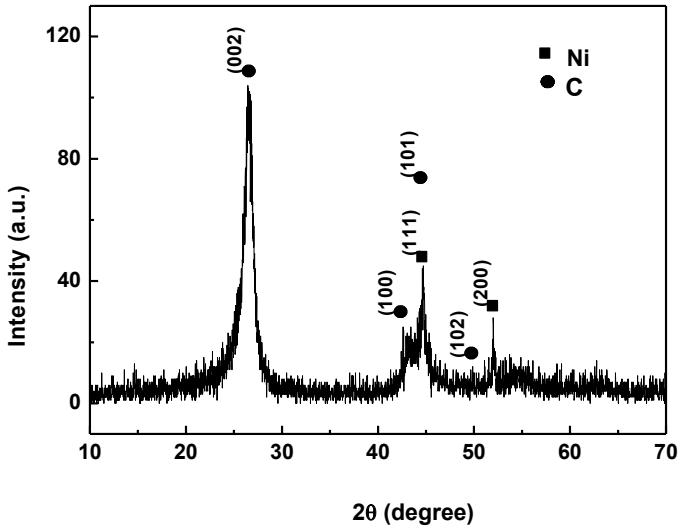

Fig. 3.40.(a)XRD patternof carbonnanowhisker obtained from palmolein oil

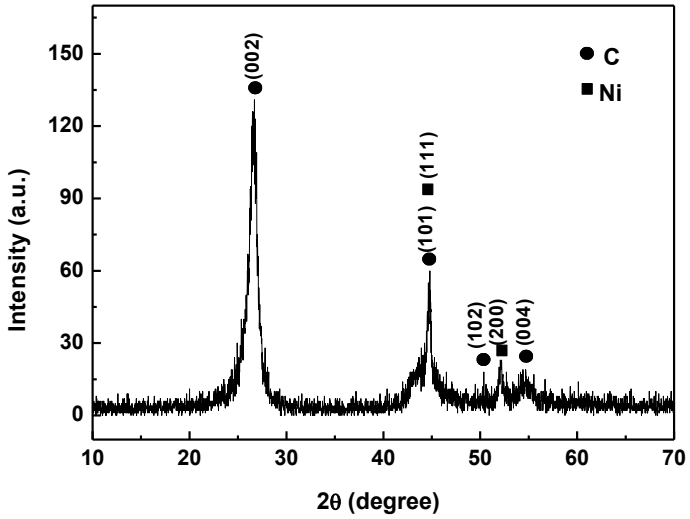

Fig. 3.40. (b) XRD pattern of carbon nanorings obtained from palmolein oil

3.10. Multiwalled carbon nanotubes(MWCNT) and nanowhiskers (CNW) from D-fructose

3.10.1. Materials

Commercially availableD-fructose has been used as precursor for the synthesis of carbon nanotubes and nanowhiskers.

3.10.2. Synthesis of carbon MWCNTs and CNWs from D-fructose

The MWCNTs and CNWs were prepared in separate experiments from D-fructose using nickel nanoparticles as catalyst by varying the CVD temperature.

General procedure:

A quartz boat loaded with fructose (~10 g) was kept in a lower-temperature zone (300^0C) and another quartz boat in which 1mg of nickel nanoparticles previously dispersed uniformly using ethanol was kept at a higher temperature zone (650^0C for MWCNTs and 550^0C for CNWs) in the horizontal quartz tube in CVD furnace. Argon gas was then purged at a rate of 6cm^3/min. The desired temperature was maintained for 2 hours and then allowed to cool to ambient temperature whereupon the respective products were obtained. The catalyst particles were removed by washing with mild acid solution. The yieldwas recorded to be ~2.9 g and ~3.0 g, respectively.

3.10.3. Results and discussion

The materialswereobtained in relatively good yield (~30%). The diversity in morphology was achieved by varying the CVD temperature. Notably, a higher temperature favoured the formation nanotubes. It is noteworthy that D-fructose when subjected to catalyst free CVD process under similar conditions afforded diamond like carbon(DLC) only.

3.10.3.1. Scanning electron microscopy andtransmission electron microscopy of MWCNT

The SEM micrographs (**Fig.3.41(a,b)**) of the as-obtained material from D-fructose using catalyst revealed bundles of nanotubes. The TEM micrographs (**Fig.3.41 (c)**) showed micrometer long hollow structure of nanotubes. The HRTEM image(**Fig.3.41 (d,e)**) showed that the outer and inner diameters of the nanotubes were 20 and 6 nm, respectively with an open end. HRTEM also suggested that the as-grown nanotubes to be consisting of concentrically nested ~19 graphene sheets. The interlayer distance is about 0.33 nm which resembles that of (002) plane of the graphitic carbon. The SAED pattern(**Fig.3.41 (f)**)indicated poly crystalline nature of the material.

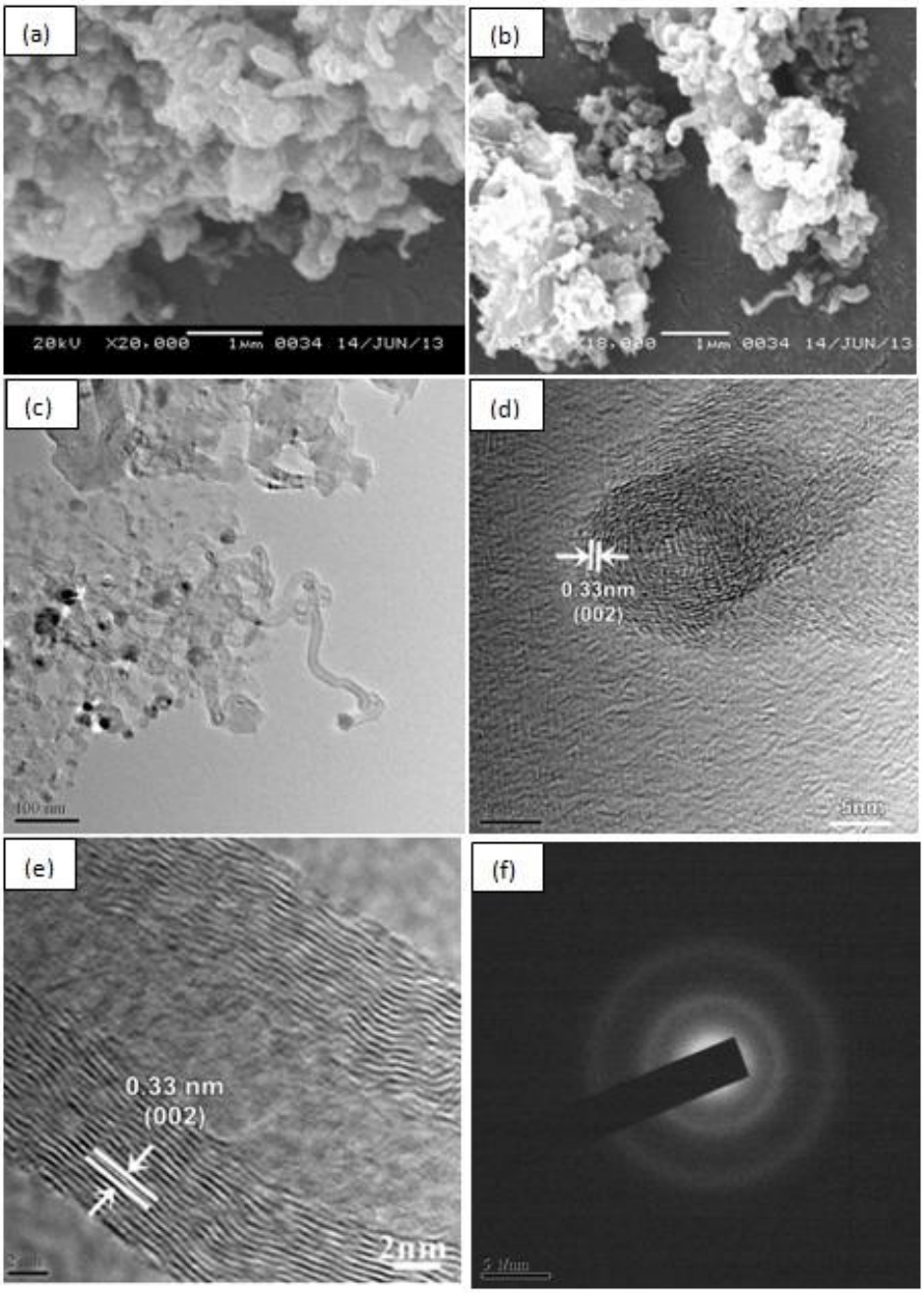

Fig.3.41. (a,b) SEM micrograps **(c)** TEM micrograph **(d,e)** HRTEM micrograph**(f) SA**EDpattern of MWCNT obtained from D-fructose

3.10.3.2.Scanning electron microscopy and transmission electron microscopy of CNW from D-fructose

The SEM micrographs (**Fig.3.42 (a,b))** showed the presence of agglomerated carbon nanowhiskers. The TEM images (**Fig.3.42(c,d))** also revealed the presence of nanowhiskers. The HRTEM indicated the graphitized nature of the whiskers. The carbon spirals in the whiskers indicated by black arrows (**Fig.3.42 (e)).** The interlayer

distance is about 0.34 nm which resembles that of (002) plane of the graphitic carbon. The SAED pattern **(Fig.3.42 (f))** revealed systematic rings that are characteristic of poly crystalline nature of the material.

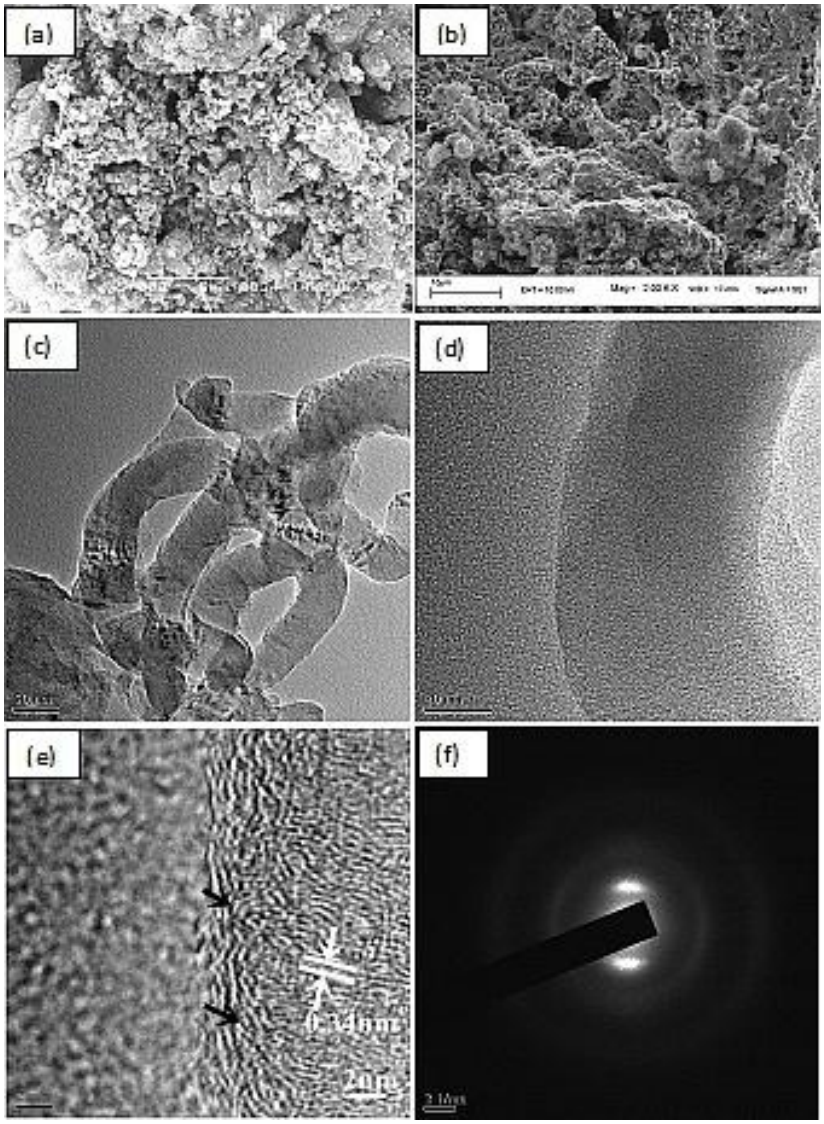

Fig.3.42. (a,b) SEM micrographs **(c,d)** TEM micrographs **(e)** HRTEM micrograph**(f)** SAED pattern of CNW obtained from D-fructose

3.10.3.3. XRD analysis and EDS analysis of MWCNTfrom D-fructose

The powder XRD pattern**(Fig.3.43)** exhibited intense and sharp peaks that were assigned toBragg reflections from graphitic carbon and nickel nanoparticles. The peaks at 2θ values 44.29^0 and 51.83^0 correspond to the (111) and (200) crystallographic planes of face centered cubic nickel (JCPDS file no.04-0850) and peaks at 26.62^0, 44.63^0, 51.97^0 of 2θ values correspond to the (002), (101) and (102)

crystallographic planes of hexagonal graphitic carbon (JCPDS file no. 23-0064). The average crystallite size estimated to be 15.9 nm for (002) plane of graphite.

The Energy dispersive spectrum (EDS) (**Fig.3.44**) of the sample attested the presence of carbon and nickel which is concordant with X-ray diffraction findings.

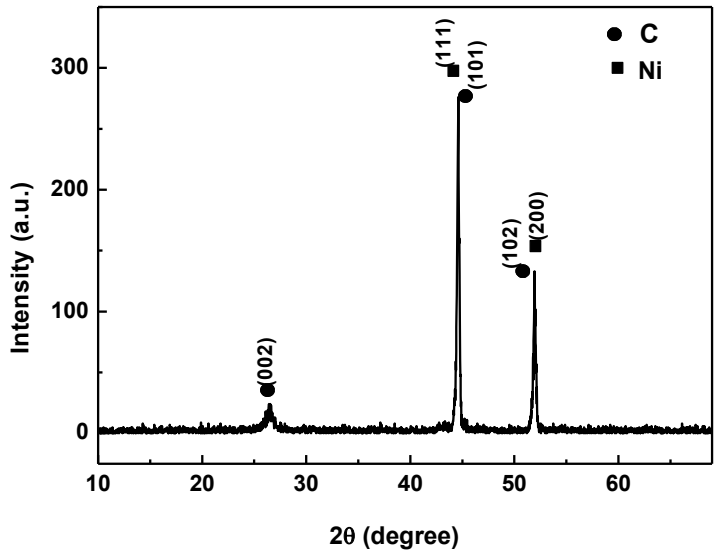

Fig.3.43. XRD pattern of MWCNTobtained from D-fructose

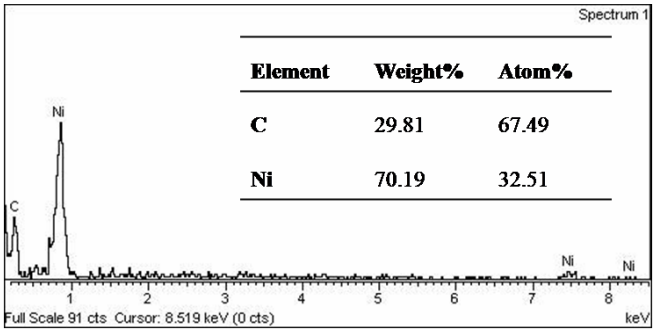

Fig.3.44.EDS of MWCNT obtained from D-fructose

3.10.3.4. XRD analysis and EDS analysis of CNW from D-fructose

The**Fig.3.45** exhibited the XRD pattern of synthesizedCNW from fructose. The peaks were indexed to the fccnickel (JCPDS file no.04-0850) and hexagonal graphitic carbon (JCPDS file no. 23-0064). The average crystallite size estimated by the Debye-Scherrer equation using a Gaussian fit was found to be 14.0 nm.

The Energy dispersive spectrum (EDS) of the sample obtained by CVD of fructose at 550^0 C shown in (**Fig.3.46**), revealed the presence of carbon and nickel in the sample. Thepresence of oxygen is also evident from the result.

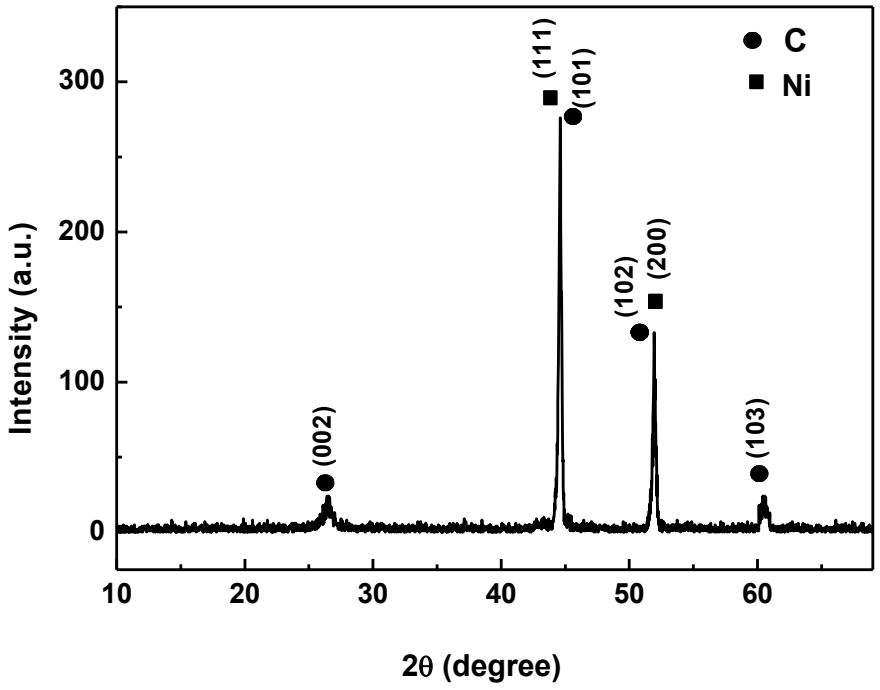

Fig.3.45.XRD pattern of CNWobtained from D-fructose

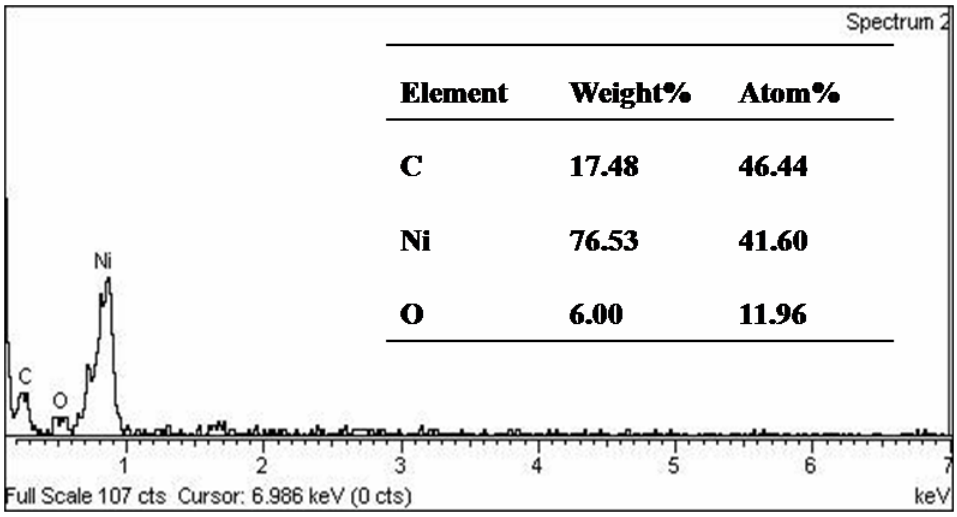

Fig.3.46.EDS of CNWobtained from D-fructose

3.11. Multiwalled carbon nanotubes (MWCNT)and carbon nanowhiskers(CNW) from 1-butanol

3.11.1. Materials

Analytical reagent grade 1-butanol is used as precursor for the synthesis of CNW and MWCNT.

3.11.2. Synthesis of CNW and MWCNT

The CNWs and MWCNTs were prepared in two separate experiments by CVD method from 1-butanol under catalytic condition using Ni and Co nanoparticles as catalyst, respectively.

General procedure:A quartz boat loaded with 1- butanol (10 g) was kept in a lower-temperature zone (300°C) and another quartz boat in which 1mg of Ni nanoparticles (for CNWs) or Co nanoparticles (for MWCNTs) previously dispersed uniformly using ethanol was kept at a higher temperature zone (750°C) in the horizontal quartz tube of CVD apparatus. Argon gas was then purged at a rate of $6cm^3$/min. The furnace was heated to 750^0C at a rate of 7^0C /min for 2 hours and then allowed to cool to ambient temperature whereupon the CNWs and MWCNTs were obtainedin respective boatsas black powder. The yieldwas recorded to be ~2.8 g and ~3.2g, respectively.

3.11.3. Results and discussion

The material was obtained in relatively good yield (~30%). The temperature and catalyst played a crucial role in dictating the morphology of the as-formed materials.The presence of cobalt nanoparticles as catalyst, MWCNTs were formed while in presence of nickel nanoparticles, CNWs were obtained. Temperature below 750^0 C yielded agglomerated product. The catalyst free chemical vapour deposition of butanol ended with glassy carbon.

It is noteworthy from literature that aliphatic alcohols including butanol as carbon precursorwere subjected to spray pyrolysis at 700 to 900^0C.No carbon nanotubes were formed at 700^0C and from 850 to 900^0C, graphiteformation was noticed. Conducive condition for the nanotubes wasin the range 750-800^0C [127].

3.11.3.1. (a) Scanning electron microscopy andtransmission electron microscopy of CNWfrom 1-butanol

The SEM micrographs (**Fig.3.47 (a)**) of the as-obtained material from 1- butanol using nickel catalystrevealed agglomeratednanowhiskers. The TEM micrographs (**Fig.3.47 (b)**) also indicated the presence of nanowhiskers. The HRTEM image (**Fig.3.47(c)**) showed that the lattice fringes between the two adjacent planes are 0.33nm apart, which is equal to the interlayer distance of (002) plane of the graphitic carbon. The SAED pattern (**Fig.3.47 (d)**) revealed defused concentric rings that are characteristic of graphitic carbon.

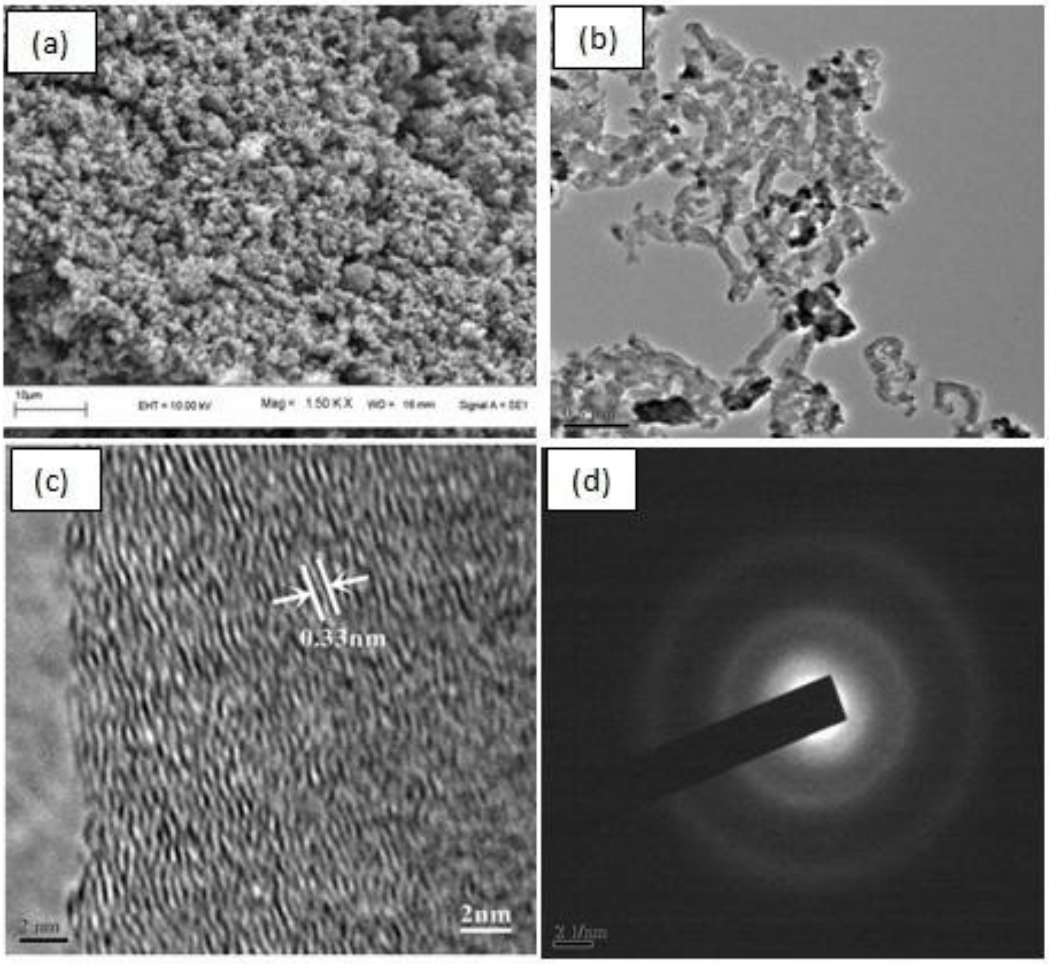

Fig.3.47. (a) SEM micrograph **(b)** TEM micrograph **(c)** HRTEM micrograph**(d)**SAED patternof the material obtained from 1-butanol

3.11.3.1. (b) Scanning electron microscopy andtransmission electron microscopy of MWCNT from 1-butanol

The SEM micrograph (**Fig.3.48 (a)**) of the as-obtained material from 1- butanol using cobalt nanoparticle as catalystrevealed entangled noodle-like densely packed multi walled carbon nanotubes. The TEM micrographs (**Fig.3.48 (b)**) indicated the presence of clean hollow and intertwined nanotubes of length more than 10μm. The HRTEM image (**Fig.3.48 (c)**) showed that the as-grown nanotubes to be consisting of concentrically nested ~ 14 graphene cylinders. The inner and outer diameter of the tube wasfound to be 4nm and 17nm respectively. The interlayer distance is about 0.36 nm which resembles that of (002) plane of the graphitic carbon. The SAED(**Fig. 3.48 (d)**) revealed concentric rings that are characteristic of graphitic carbon.

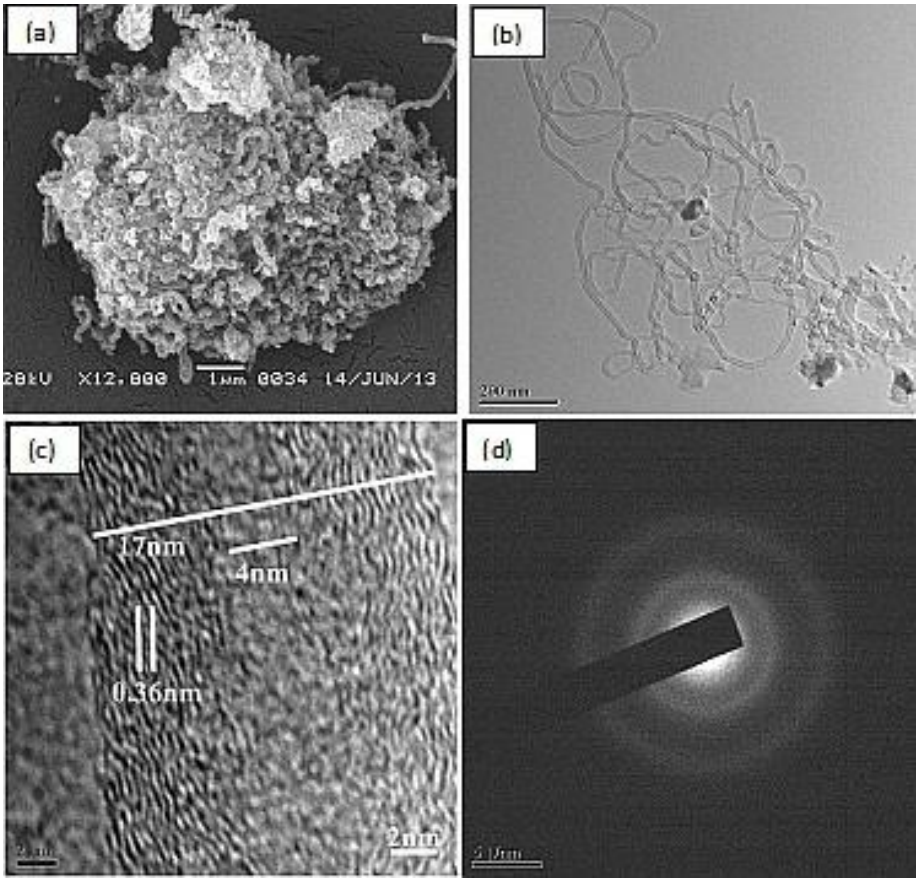

Fig.3.48. (a) SEM micrograph **(b)** TEM micrograph **(c)** HRTEM micrograph**(d)** SAED pattern of MWCNT from 1-butanol

In contrast to the MWCNTs obtained from renewable natural oils(65-18) and fats (25) containing fatty acids (vide supra), the number of graphene walls got reduced in case of butanol (14) having only -OH functions. Use of ferrocene catalyst further reduced

the number of walls (6) of MWCNT obtained by nebulised spray pyrolysis method at 750^0C[127].

3.11.3. 2. XRD analysis of CNW using nickel nanoparticles as catalyst

The XRD pattern **(Fig.3.49)** exhibited a number of intense and sharp peaks assigned toBragg reflections from both graphitic carbon and nickel. The peaks at 44.57^0 and 51.90^0 of 2θ were indexed to the (111) and (200) crystallographic planes of face centered cubic nickel (JCPDS file no.04-0850) and peaks at 26.61^0, 44.41^0,51.59^0 of 2θ values were indexed to be (002), (101) and (102) crystallographic planes of hexagonal graphitic carbon (JCPDS file no. 23-0064). The average crystallite size estimated by the Debye-Scherrer equation using a Gaussian fit was found to be13.1 nm.

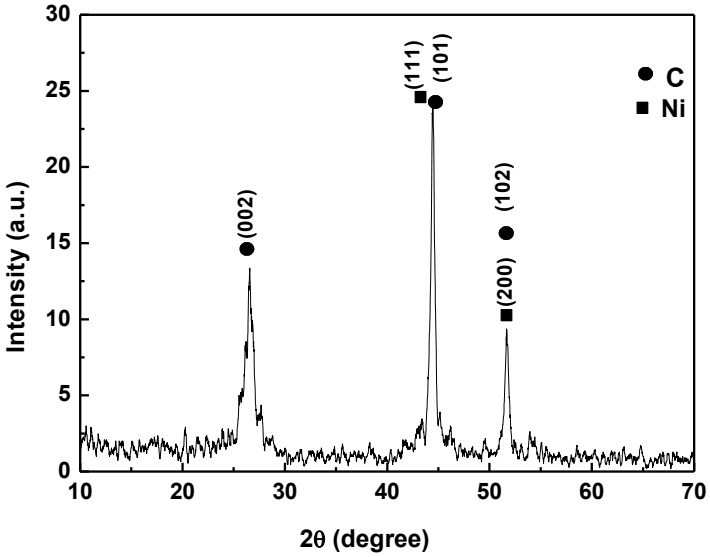

Fig.3.49. XRD pattern of the CNW obtained using Ni catalyst from 1-butanol

3.11.3.3. XRD analysis and EDS analysis of MWCNT using cobaltnanoparticles as catalyst from 1-butanol

The X-ray diffraction pattern**(Fig.3.50)** showed peaks (44.29° and 46.17°) of 2θ values which correspond to the (002) and (101) crystallographic planes of hexagonalphase of cobalt (JCPDS file no.89-4308) and peaks (26.69°, 44.46°, 51.80°) of 2θ values correspond to the (002), (101) and (102) crystallographic planes of hexagonal graphitic carbon (JCPDS file no. 23-0064). The average crystallite size

estimated by the Debye -Scherrer equation using a Gaussian fit was found to be 11.1nm for (002) peak of carbon.It is pertinent here to mention that the clean, long and regular shaped nanotubes obtained using Co nanoparticle as catalyst during chemical vapour deposition process of 1-butanol.

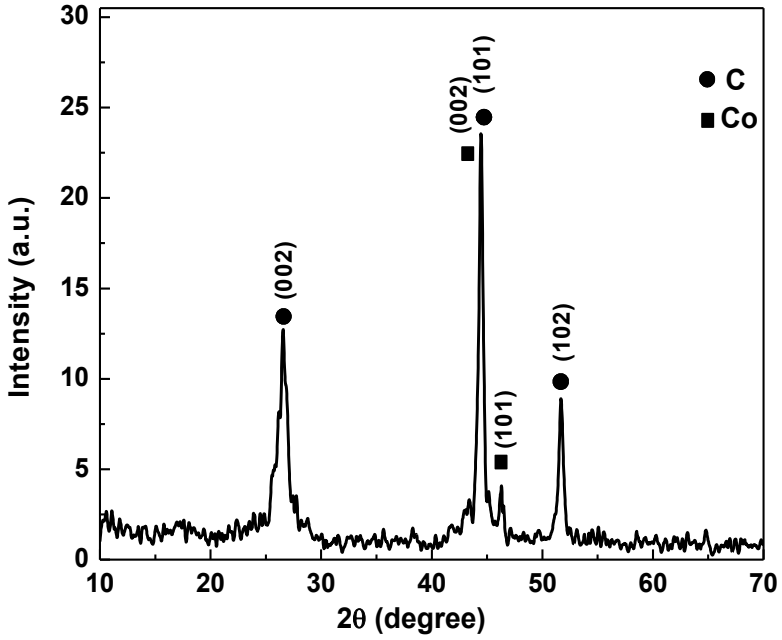

Fig.3.50.XRD pattern of MWCNT obtained from 1-butanol using Co catalyst

The Energy dispersive spectrum (EDS) of the material obtained butanolusing cobalt nanoparticles as catalyst(**Fig.3.51**), revealed the presence of carbon and cobalt in the sample. Thepresence of oxygen was also evident from the result.

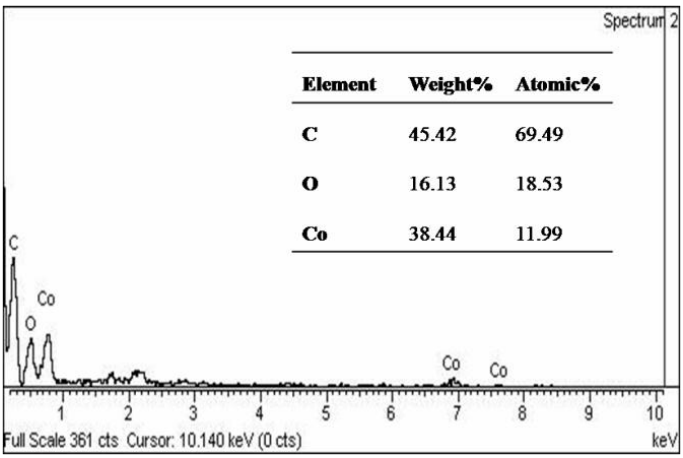

Fig.3.51.EDS of MWCNT from 1-butanolusing cobalt nanoparticles as catalyst

3.12. Multiwalled carbon nanotubes (MWCNT) from vinyl alcohol

3.12.1. Materials

Analytical grade vinyl alcohol was used as precursor for the synthesis of MWCNT.

3.12.2. Synthesis of MWCNT

The MWCNTs were prepared by CVD method from vinyl alcohol using nickel nanoparticles as catalyst. The synthetic procedure was similar that mentioned in the section 3.3.2 of this chapter. The furnace was heated to 750^0C at a rate of 7^0C /min for 2 hours and then allowed to cool to ambient temperature whereupon the MWCNTs were obtained as black powder (yield ~3 g).

3.12.3. Results and discussion

The as obtainedmaterial was black, amorphous and highly dispersive in aqueous and organic solvents under ultrasonication. The yield was recorded to be 30% of the initial mass.

3.12.3.1. Scanning electron microscopy andtransmission electron microscopy of MWCNT

The SEM micrographs (**Fig.3.52 (a,b)**) of the as-obtained material from vinyl alcohol using nickel catalystrevealed bundles of nanotubes. The TEM micrographs (**Fig. 3.52 (c,d)**) indicated the presence of micrometer long multiwalled nanotubes. The HRTEM image (**Fig. 3.52(e)**) showed that the as-grown nanotubes to be consisting of concentrically nested ~ 22 graphene sheets. The inner and outer diameters were found to be 5.0 nm and 20.7 nmrespectively. The interlayer distance is about 0.33 nm which resembles that of (002) plane of the graphitic carbon. The SAED pattern (**Fig. 3.52 (f)**) revealed concentric rings that are characteristic of graphitic carbon.

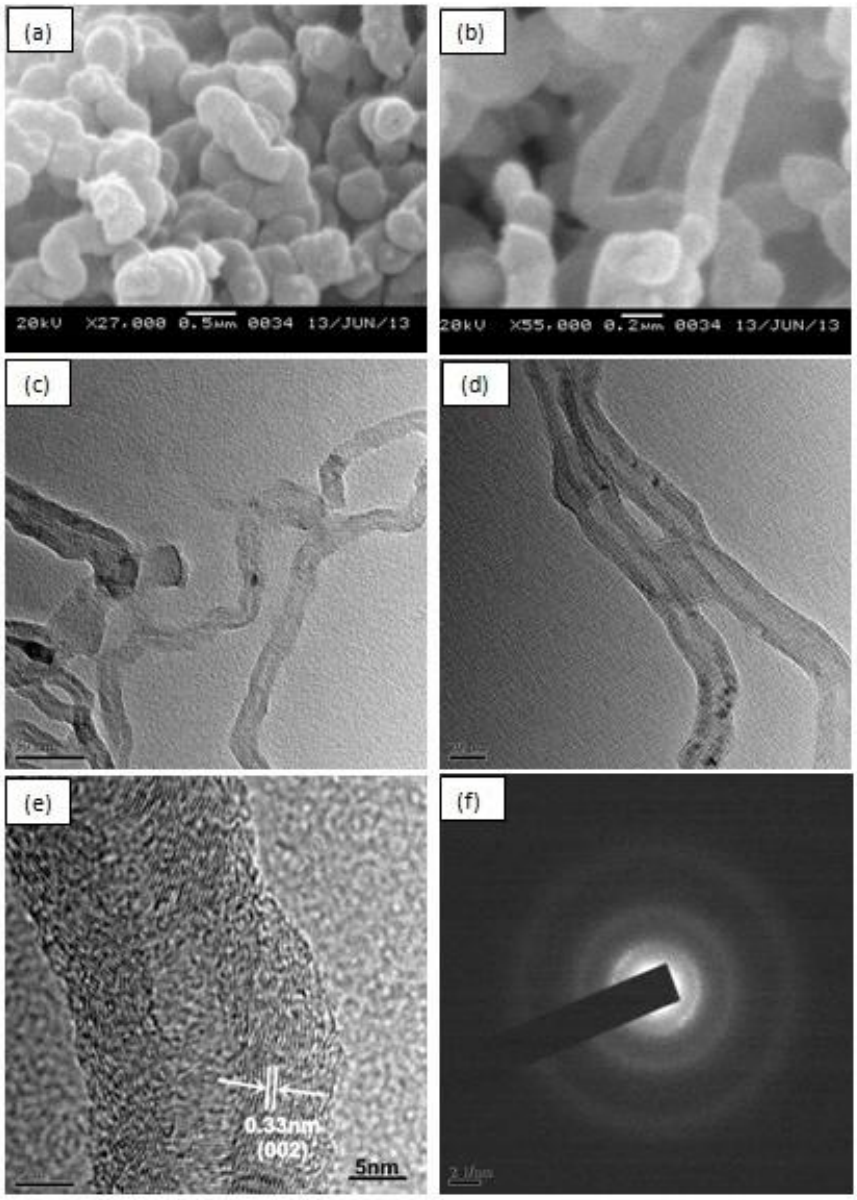

Fig.3.52. (a,b) SEM micrographs **(c,d)** TEM micrographs **(e)** HRTEM micrograph **(f)** SAED pattern of MWCNT obtained from vinyl alcohol

3.12.3.2. X-ray diffractionstudy of MWCNT from vinyl alcohol

The XRD pattern**(Fig.3.53)** of as-obtained materialexhibited a number of intense and sharp peaks assigned toBragg reflections from both graphitic carbon and nickel. The X-ray diffraction pattern showed peaks (44.71° and 51.74°) of 2θ values ranging from 10^0 to 70^0, which correspond to the (111) and (200) crystallographic planes of fcc Ni (JCPDS file no.04-0850) and peaks (26.59^0, 44.71^0,51.74^0) of 2θ values also correspond to the (002), (101) and (102) crystallographic planes of hexagonal

graphitic carbon (JCPDS file no. 23-0064). The average crystallite size estimated by the Debye-Scherrer equation using a Gaussian fit was found to be 8.0 nm.

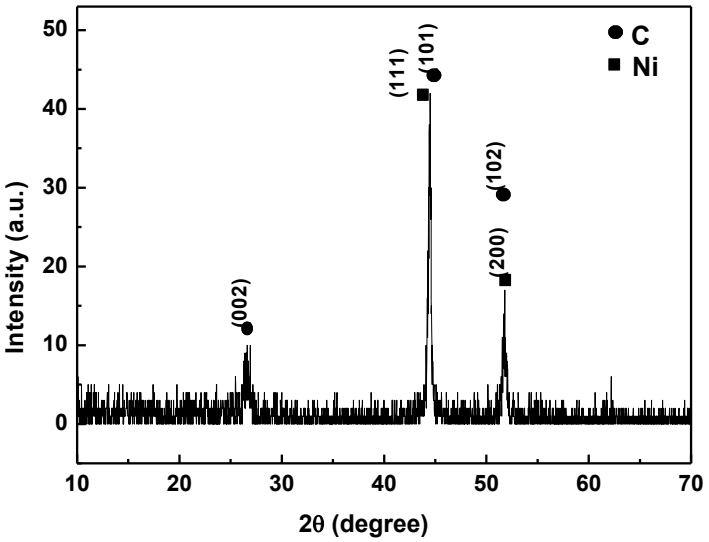

Fig.3.53. XRD pattern of the materials obtained from vinyl alcohol

References

[1] Iijima, S. *Nature*, 1991, **354**, 56.

[2] Falvo, M. R., Clary, G. J., Taylor, R. M., Chi, V., Brooks, F. P., Washburn, S., & Superfine, R. *Nature*, 1997, **389**, 582.

[3] Coleman, J. N., Khan, U., Blau, W. J., & Gunko, Y. K. *Carbon*, 2006, **44**, 1624.

[4] Iijima, S., Brabec, C., Maiti, A., & Bernholc, J.*J. Chem. Phys*, 1996, **104**, 2089.

[5] Krishnan, A., Dujardin, E., Ebbesen, T. W., Yianilos, P. N., & Treacy, M. M. J. *Phys. Rev. B*, 1998, **58**, 14013.

[6] Lourie, O., Cox, D. M., & Wagner, H. D.*Phys. Rev. Lett*., 1998, **81**, 1638.

[7] Lu, J. P. *Phys. Rev. Lett*, 1997, **79**, 1297.

[8] Nardelli, M. B., Yakobson, B. I., & Bernholc, J. *Phys. Rev. Lett.*,1998, **81**, 4656.

[9] Qian, D., Wagner, G. J., Liu, W. K., Yu, M. F., & Ruoff, R. S, *Appl.Mech. Rev.*, 2002, **55**, 495.

[10] Guo, J., Liu, Y., Prada-Silvy, R., Tan, Y., Azad, S., Krause, B., & Grady, B. P.*J. Polym. Sci. Pol. Phys.*, 2014, **52**, 73.

[11] Salvetat, J. P., Briggs, G. A. D., Bonard, J. M., Bacsa, R. R., Kulik, A. J., Stockli, T., & Forró, L. *Phys. Rev. Lett.*, 1999, **82**, 944.

[12] Treacy, M. J., Ebbesen, T. W., & Gibson, J. M. *Nature*, 1996, **381**, 678.

[13] Wong, E. W., Sheehan, P. E., & Lieber, C. M. *Science*, 1997, **277**, 1971.

[14] Wang, Q.H., Bellisario, D.O., Drahushuk, L.W., Jain, R.M., Kruss, S., Landry, M.P., Mahajan, S.G., Shimizu, S.F., Ulissi, Z.W. & Strano, M.S.*Chem. Mater.*, 2013, **26**,172.

[15] Yu, M. F., Lourie, O., Dyer, M. J., Moloni, K., Kelly, T. F., & Ruoff, R. S. *Science*, 2000, **287**, 637.

[16] Han, Z., & Fina, A. *Prog. Polym. Sci.*, 2011, **36**, 914.

[17] Benedict, L. X., Louie, S. G., & Cohen, M. L. *Solid State Commun.*,1996, **100**, 177.

[18] Chiu, H. Y., Deshpande, V. V., Postma, H. W.C., Lau, C.N., Miko, C, Forro, L., &Bockrath, M. *Phys. Rev. Lett*, 2005, **95**, 226101.

[19] Aliev, A. E., Lima, M. H., Silverman, E. M., & Baughman, R. H. *Nanotechnology*,2009, **21**, 035709.

[20] Marconnet, A. M., Panzer, M. A., & Goodson, K. E. *Rev. Mod. Phys.*, 2013, **85**, 1295.

[21] Jakubinek, M.B., Johnson, M.B., White, M.A., Jayasinghe, C., Li, G., Cho, W., Schulz, M.J. & Shanov, V. *Carbon*, 2012, **50**, 244.

[22] Hone, J., Llaguno, M. C., Biercuk, M. J., Johnson, A. T., Batlogg, B., Benes, Z., & Fischer, J. E. *Appl. Phys. A*, 2002, **74**, 339.

[23] Pradhan, N. R., Duan, H., Liang, J., & Iannacchione, G. S. *Nanotechnology*, 2009, **20**, 245705.

[24] Huxtable, S. T., Cahill, D. G., Shenogin, S., Xue, L., Ozisik, R., Barone, P., & Keblinski, P.*Nat. Mater.*, 2003, **2**, 731.

[25] Kim, P., Shi, L., Majumdar, A., & McEuen, P. L. *Phys. Rev. Lett.*, 2001, **87**, 215502.

[26] Maniwa, Y., Fujiwara, R., Kira, H., Tou, H., Kataura, H., Suzuki, S., & Fujiwara, A.*Phys. Rev. B.*, 2001, **64**, 241402.

[27] Mingo, N., & Broido, D. A. *Phys. Rev. Lett.*, 2005, **95**, 096105.

[28] Pop, E., Mann, D., Wang, Q., Goodson, K., & Dai, H. *Nano Lett.*, 2006, **6**, 96.

[29] Zhang, Q., Chen, G., Yoon, S. F., Ahn, J., Wang, S. G., Zhou, Q., & Li, J. Q. *Phys. Rev. B.*, 2002, **66**, 165440.

[30] Avouris, P., Chen, Z., & Perebeinos, V.*Nat. Nanotechnol.*, 2007, **2**, 605.

[31] Blase, X., Benedict, L. X., Shirley, E. L., & Louie, S. G. *Phys. Rev. Lett.*, 1994, **72**, 1878.

[32] Bockrath, M., Cobden, D. H., McEuen, P. L., Chopra, N. G., Zettl, A., Thess, A., & Smalley, R. E. *Science*, 1997, **275**, 1922.

[33] Dai, H., Wong, E. W., & Lieber, C. M. *Science*, 1996, **272**, 523.

[34] Derycke, V., Martel, R., Appenzeller, J., & Avouris, P. *Nano Lett.*, 2001, **1**, 453.

[35] Ebbesen, T. W., Lezec, H. J., Hiura, H., Bennett, J. W., Ghaemi, H. F., & Thio, T. *Nature*, 1996, **382**, 54.

[36] Hamada, N., Sawada, S. I., & Oshiyama, A. *Phys. Rev. Lett.*, 1992, **68**, 1579.

[37] Jishi, R. A., Dresselhaus, M. S., & Dresselhaus, G.*Phys. Rev. B.*, 1993, **48**, 11385.

[38] Lambin, P., Fonseca, A., Vigneron, J. P., Nagy, J. B., & Lucas, A. A. *Chem. Phys. Lett.*, 1995, **245**, 85.

[39] Mintmire, J. W., Dunlap, B. I., & White, C. T. *Phys. Rev. Lett.*, 1992, **68**, 631.

[40] Ouyang, M., Huang, J. L., Cheung, C. L., & Lieber, C. M. *Science*, 2001, **292,** 702.

[41] Saito, R., Dresselhaus, G., & Dresselhaus, M. S. *Phys. Rev. B.*, 1996, **53**, 2044.

[42] Saito, R., Fujita, M., Dresselhaus, G., & Dresselhaus, U. M. *Appl. Phys. Lett.*, 1992, **60**, 2204.

[43] Tang, Z. K., Zhang, L., Wang, N., Zhang, X. X., Wen, G. H., Li, G. D., & Sheng, P. *Science*, 2001, **292**, 2462.

[44] Yao, Z., Postma, H. W. C., Balents, L., & Dekker, C. *Nature*, 1999, **402**, 273.

[45] Ajayan, P. M., Terrones, M., De la Guardia, A., Huc, V., Grobert, N., Wei, B. Q., & Ebbesen, T. W. *Science*, 2002,**296**, 705.

[46] Bachtold, A., Hadley, P., Nakanishi, T., & Dekker, C. *Science*, 2001, **294**, 1317.

[47] Collins, P. G., Arnold, M. S., & Avouris, P. *Science*, 2001, **292**, 706.

[48] Klinke, C., Hannon, J. B., Afzali, A., & Avouris, P. *Nano Lett.*, 2006, **6**, 906.

[49] Koswatta, S. O., Perebeinos, V., Lundstrom, M. S., & Avouris, P. *Nano Lett.*, 2008, **8**, 1596.

[50] Lin, Y. M., Appenzeller, J., Knoch, J., Chen, Z., & Avouris, P. *Nano Lett.*, 2006, **6**, 930.

[51] Gooding, J. J. *Electrochim. Acta.*, 2005, **50**, 3049.

[52] Gong, K., Chakrabarti, S., & Dai, L. *Angew. Chem.*, 2008, **47**, 5446.

[53] Lee, N. S., Chung, D. S., Han, I. T., Kang, J. H., Choi, Y. S., Kim, H. Y., & Jung, J. E. *Diam. Relat. Mater.*, 2001, **10**, 265.

[54] Balasubramanian, K., & Burghard, M. *J. Mater. Chem.*, 2008, **18**, 3071.

[55] Chopra, S., Pham, A., Gaillard, J., Parker, A., & Rao, A. M. *Appl. Phys. Lett.*, 2002, **80**, 4632.

[56] Lerner, M.B., Matsunaga, F., Han, G.H., Hong, S.J., Xi, J., Crook, A., Perez-Aguilar, J.M., Park, Y.W., Saven, J.G., Liu, R. & Johnson, A.C. *Nano Lett.*, 2014, **14**, 2709.

[57] Lerner, M. B., Resczenski, J. M., Amin, A., Johnson, R. R., Goldsmith, J. I., & Johnson, A. C. *J. Am. Chem. Soc.*, 2012, **134**, 14318.

[58] Lerner, M. B., Goldsmith, B. R., McMillon, R., Dailey, J., Pillai, S., Singh, S. R., & Johnson, A. C. *AIP Adv.*, 2011, **1**, 042127.

[59] Kong, J., Chapline, M. G., & Dai, H. *Adv. Mater.*, 2001, **13**, 1384.

[60] Kong, J., Franklin, N. R., Zhou, C., Chapline, M. G., Peng, S., Cho, K., & Dai, H. *Science*, 2000, **287**, 622.

[61] Riemenschneider, J., Temmen, H., & Monner, H. P. *J. Nanosci.Nanotechnol*.,2007, **7**, 3359.

[62] Varghese, O. K., Kichambre, P. D., Gong, D., Ong, K. G., Dickey, E. C., & Grimes, C. A. *Sensor Actuat. B-Chem.*, 2001, **81**, 32.

[63] Wong, S. S., Joselevich, E., Woolley, A. T., Cheung, C. L., & Lieber, C. *Nature*, 1998, **394**, 52.

[64] Vardharajula, S., Ali, S. Z., Tiwari, P. M., Eroğlu, E., Vig, K., Dennis, V. A., & Singh, S. R. *Int. J. Nanomedicine*, 2012, **7**, 5361.

[65] Liu, Z., Tabakman, S., Welsher, K., & Dai, H. *Nano Res.*, 2009, **2**, 85.

[66] Alturaif, H. A., Alothman, Z. A., Shapter, J. G., & Wabaidur, S. M. *Molecules*, 2014, **19**, 17329.

[67] Wang, F., Kozawa, D., Miyauchi, Y., Hiraoka, K., Mouri, S., Ohno, Y., & Matsuda, K. *Nat. Commun.*, 2015, 6, 1.

[68] Tsuboi, Y., Wang, F., Kozawa, D., Funahashi, K., Mouri, S., Miyauchi, Y., & Matsuda, K. *Nanoscale*, 2015, **7**, 14476.

[69] Chambers, A., Park, C., Baker, R. T. K., & Rodriguez, N. M. *J. Phys. Chem.B*, 1998, **102**, 4253.

[70] Dai, G. P., Liu, C., Liu, M., Wang, M. Z., & Cheng, H. M. *Nano Lett.*, 2002, **2**, 503.

[71] Lee, S. M., An, K. H., Lee, Y. H., & Seifert, G. *J. Am. Chem. Soc*, 2001, **123**, 5059.

[72] Meregalli, V., Parrinello, M. *Appl. Phys. A*, 2001, **72**, 143.

[73] Liu, C., Fan, Y. Y., Liu, M., Cong, H. T., Cheng, H. M., & Dresselhaus, M. S. *Science,* 1999, **286**, 1127.

[74] Lee, S. M., & Lee, Y. H. *Appl. Phys. Lett.*, 2000, **76**, 2877.

[75] Bajwa, N., Li, X., Ajayan, P. M., & Vajtai, R. *J. Nanosci.Nanotechnol.*,2008, **8**, 6054.

[76] Halonen, N., Kordas, K., Toth, G., Mustonen, T., Maklin, J., Vahakangas, J., Vajtai, R. *J. Phys. Chem.C*, 2008, **112**, 6723.

[77] Wei, B. Q., Vajtai, R., Jung, Y., Ward, J., Zhang, R., Ramanath, G., &Ajayan, P. M. *Chem. Mater.*, 2003, **15**, 1598.

[78] Wei, B. Q., Ward, J. W., Vajtai, R. A. A., Ajayan, P. M., Ma, R., & Ramanath, G. *Chem. Phys. Lett.*2002, **354**, 264.

[79] Wei, B. Q., Vajtai, R., & Ajayan, P. M. *Carbon*, 2003, **41**, 185.

[80] Shah, K. A., & Tali, B. A. *Mater. Sci. Semicond. Process.*, 2016, **41**, 67.

[81] Kumar, M., & Ando, Y.*J. Nanosci. Nanotechnol.*,2010, **10**, 3739.

[82] Terrones, M. Annu. *Rev. Mater. Res*., 2003, **33**, 419.

[83] Afre, R. A., Soga, T., Jimbo, T., Kumar, M., Ando, Y., Sharon, M., & Umeno, M. *Micro. Mesop. Mat.* 2006, **96**, 184.

[84] Kumar, M., & Ando, Y. *Carbon*, 2005, **43**, 533.

[85] Afolabi, A. S., Abdulkareem, A. S., & Iyuke, S. E. *J. Exp. Nanosci.* 2007, **2**, 269.

[86] Afre, R. A., Soga, T., Jimbo, T., Kumar, M., Ando, Y., & Sharon, M. *Chem. Phys. Lett.*, 2005, **414**, 6.

[87] Ghosh, P., Soga, T., Afre, R. A., & Jimbo, T. *J. Alloy Compd.*, 2008, **462**, 289.

[88] Suriani, A. B., Dalila, A. R., Mohamed, A., Mamat, M. H., Salina, M., Rosmi, M. S., & Rusop, M. *Mater. Lett.*, 2013, **101**, 61.

[89] Suriani, A. B., Azira, A. A., Nik, S. F., Nor, R. M., & Rusop, M. *Mater. Lett.* , 2009, **63**, 2704.

[90] Dai, H. *Acc. Chem. Res.*, 2002, **35**, 1035.

[91] Fenoglio, I., Greco, G., Tomatis, M., Muller, J., Raymundo-Pinero, E., Béguin, F., & Fubini, B. *Chem. Res. Toxicol.*, 2008, **21**, 1690.

[92] Galano, A. *Nanoscale*, 2010, **2**, 373.

[93] Homma, Y., Kobayashi, Y., Ogino, T., Takagi, D., Ito, R., Jung, Y. J., & Ajayan, P. M. *J. Phys. Chem. B*, 2003, **107**, 12161.

[94] Rajesh, J. A., & Pandurangan, A. *RSC Adv.*, 2014, **4**, 20554.

[95] Tripathi, S., Sharon, M., Malder, N. N., Shukla, J., & Sharon, M. *Arch. Appl. Sci. Res.*, 2012,**4**, 1788.

[96] Stancu, M., Ruxanda, G., Ciuparu, D., & Dinescu, A. *Optoelectron. Adv. Mat*., 2011, **5**, 846.

[97] Ghosh, P., Soga, T., Tanemura, M., Zamri, M., Jimbo, T., Katoh, R., & Sumiyama, K. *Appl. Phys. A*, 2009, **94**, 51.

[98] Afre, R. A., Soga, T., Jimbo, T., Kumar, M., Ando, Y., Sharon, M., & Umeno, M. *Micro. Mesop. Mat.*, 2006, **96**, 184.

[99] Pełech, I., Owodzin, K., & Narkiewicz, U. *Annales UMCS Chemia.*,2010, **65**, 20.

[100] Lau, K. T., Lu, M., & Hui, D. *Compos. Part. B-Eng.*, 2006, **37**, 437.

[101] AuBuchon, J. F., Chen, L. H., Gapin, A. I., Kim, D. W., Daraio, C., & Jin, S. *Nano Lett.*, 2004, **4**, 1781.

[102] Bai, J. B. *Mater. Lett.* , 2003, **57**, 2629.

[103] Fejes, D., Németh, Z., & Hernádi, K. *React. Kinet. Catal. Lett.*, 2009, **96**, 397.

[104] Eichhorn, S. J. *Soft Matter*, 2011, **7**, 303.

[105] Datta, A., Dutta, P., Sadhu, A., Maiti, S., Bhattacharyya, S. *J. Nanopart. Res.*, 2013, **15**, 1.

[106] Durham, L. J., Wurster C. F., & Mosher, H. S. *J. Am. Chem. Soc.*, **80**, 332.

[107] Moreno, M. M., Olivares, D. M., Lopez, F. A., Adelantado, J. G., Reig, F. B. *Talanta*, 1999, **50**, 269.

[108] Kehrer Jr, V. J., & Leidheiser J. H. *J. Phys. Chem.*, 1954, 58, 550.

[109] Nordhei, C., Mathisen, K., Safonova, O., van Beek, W., & Nicholson, D. G. *J. Phys. Chem.C*, 2009, **113**, 19568.

[110] Pol, V. G., & Thiyagarajan, P. *J Environ Monit*., 2010, **12**, 455.

[111] Serpen, A., Capuano, E., Fogliano, V., & Gokmen, V. *J. Agric. Food Chem.*, 2007, **55**, 7676.

[112] Dubois, D., Kadish, K. M., Flanagan, S., & Wilson, L. J. *J. Am. Chem. Soc.*, 1991, **113**, 7773.

[113] Xie, Q., Perez-Cordero, E., & Echegoyen, L. *J. Am. Chem. Soc.*, 1992,**114**, 3978.

[114] Naik, G. H. , Priyadarsini, K. I., Satav, J. G., Banabalikar, M. M., Sohoni, P. P. , Biyani, M. K.,& Mohan, H. *Phytochemistry*, 2003,63, 97.

[115] Salernitano, E., Giorgi, L., Makris, T. D., Giorgi, R., Lisi, N., Contini, V., &Falconieri, M. *Diam. Relat. Mater.*2007, **16**, 1565.

[116] Schüler, T., & Tremel, W. *Chem. Commun.*, 2011, **47**, 5208.

[117] Theivasanthi, T., & Alagar, M.*Nano Biomed Eng.*,2011, **4**, 58.

[118] Xu, B., Wu, F., Chen, R., Cao, G., Chen, S., Wang, G., & Yang, Y. *J. Power Sources*, 2006, **158**, 773.

[119] Largeot, C., Portet, C., Chmiola, J., Taberna, P. L., Gogotsi, Y., & Simon, P. *J. Am. Chem. Soc.*, 2008, **130**, 2730.

[120] Amitha, F. E., Reddy, A. L. M., & Ramaprabhu, S. *J. Nanopart. Res.* 2009, **11**, 725.

[121] Manafi, S. A., Amin, M. H., Rahimipour, M. R., Salahi, E., Kazemzadeh, A. *Adv. Appl. Ceram.*, 2010, **109**, 25.

[122] Khani, H., & Moradi, O. *J. Nanostructure Chem.*, 2013, **3**, 73.

[123] Mote, V. D., Purushotham, Y., & Dole, B. N. *J. Theor. Appl. Phys.*, 2012, **6**, 1.

[124] Brand-Williams, W., Cuvelier, M. E., & Berset, C. *LWT-Food Sci. Technol.*, 1995, **28**, 25.

[125] Zobir, S. A. M., Abdullah, S., Zainal, Z., Sarijo, S. H., & Rusop, M., *Mater. Lett.*,2012, **78**, 205.

[126] Zobir, S. A. M., Bakar, S. A., Abdullah, S., Zainal, Z., Sarijo, S. H., Rusop, M. *J. Nanomater.*, 2012, 11.

[127] Ordonez-Casanova, E. G., Roman-Aguirre, M., Aguilar-Elguezabal, A., Espinosa-Magana, F. *Materials*, 2013, **6**, 2534.